Supporting Information

Photodetection of DNA Mismatches by Dissymmetric Ru(II) Acridine Based Complexes

Martin Gillard,[a] Baptiste Laramée-Milette,[b] Quentin Deraedt,[a] Garry S. Hanan,[b] Fredérique Loiseau,[c] Jérôme Dejeu,[c] Eric Defrancq,*[c] Benjamin Elias,*[a] and Lionel Marcélis*[a]

Table of contents

1. ABSORPTION AND EMISSION SPECTRA OF $[RU(BPY)_2NAPP]^{2+}$ 2

2. [RU(BPY)2NAPP]2+ SYNTHESIS 3

2.1. 2-aminonaphthalene 3

2.2. 1H-benzo[e]indole-1,2(3H)-dione 3

2.3. Methyl 2-amino-1-naphthoate 4

2.4. (2-aminonaphthalen-1-yl) methanol 4

2.5. 5-nitro-1,10-phenanthroline 4

2.6. 5-amino-1,10-phenanthroline 5

2.7. Naphtho[2,1-b]pyrido[3,2-f][1,7]phenanthroline (NAPP) 5

2.8. [Ru(bpy)2napp]2+ 6

3. NMR SPECTRA 7

4. HRMS DATA AND ELEMENTAL COMPOSITION 12

5. X-RAY CRYSTALLOGRAPHY OF $[RU(BPY)_2NAPP]^{2+}$ 14

6. CYCLIC VOLTAMMOGRAMS OF $[RU(BPY)_2NAPP]^{2+}$ 16

7. COMPUTATIONAL DATA 17

8. DNA LUMINESCENCE TITRATION FOR $[RU(BPY)_2NAPP]^{2+}$ 24

9. CIRCULAR DICHROISM MELTING CURVES 25

11. BIO-LAYER INTERFEROMETRY DATA 26

12. REFERENCES 27

1. Absorption and emission spectra of $[Ru(bpy)_2napp]^{2+}$

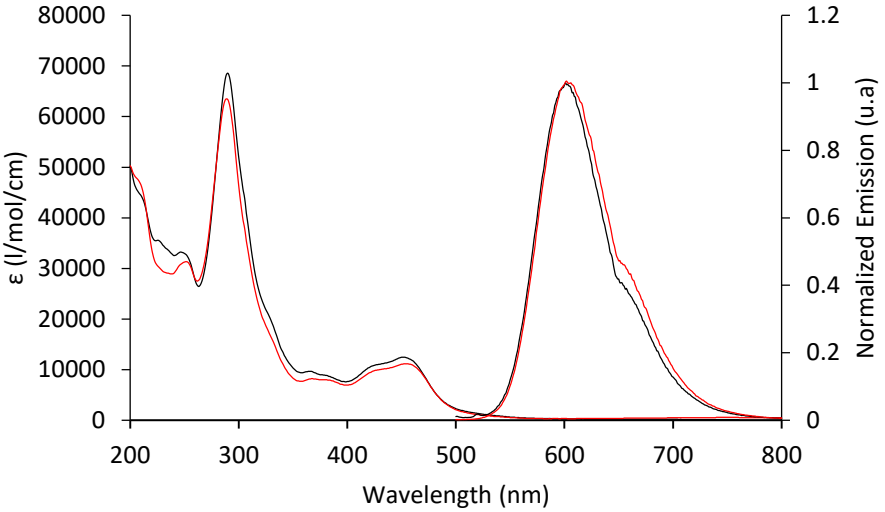

Figure S 1 Absorption and emission spectra of $[Ru(bpy)_2napp]^{2+}$ in acetonitrile (black) and in water (red) under air.

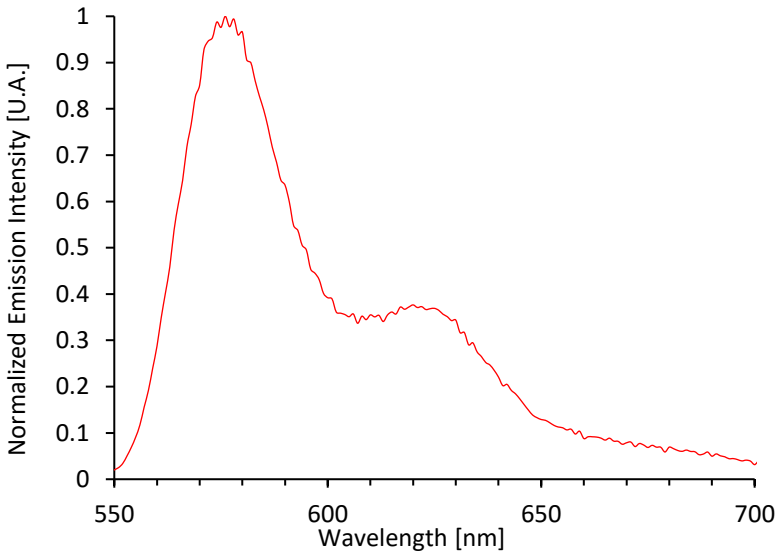

Figure S 2 Emission spectrum of $[Ru(bpy)_2napp]^{2+}$ in acetonitrile at 77 K.

2. [Ru(bpy)2napp]2+ synthesis

2.1. 2-aminonaphthalene

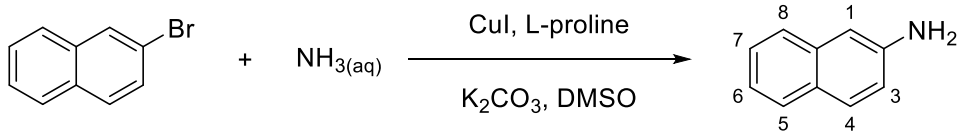

SI 1

According to a modified procedure of Ma et *al*,[1] 2-bromonaphthalene (2.94 g, 14.5 mmol, 1.0 eq.), CuI (552 mg, 2.90 mmol, 0.2 eq.), L-proline (667 mg, 5.80 mmol, 0.4 eq.), and K_2CO_3 (8.00 g, 58.0 mmol, 4.0 eq.) were placed under argon. 30 ml of deoxygenated DMSO were then added to the solids followed by 15 ml of aqueous ammonia (25%, 15 eq.). The solution was stirred at 70 °C until the bromide was consumed as monitored by TLC (18 h). The mixture was then cooled and partitioned between water and ethyl acetate and the aqueous phase was extracted two additional times with ethyl acetate. The organic phases were then combined, washed with brine, dried with Na_2SO_4 and the solvent was evaporated in vacuo to deliver a red-brown solid. This residue was finally purified by chromatography on silica gel which gave 2-aminonaphthalene **SI1** as a white solid (1.66 g, 11.6 mmol, 82%). $\mathbf{R_f}$ 0.24 (Cy /EtOAc 3 :1); **^{1}H NMR ($CDCl_3$, 300 MHz)** δ 7.72-7.63 (2H, m, ***H*$_{7\text{-}6}$**), 7.60 (d, *J* = 8.2 Hz, 1H, ***H*$_4$**), 7.59 (d, *J* = 8.2 Hz, 1H, ***H*$_3$**), 7.25-7.19 (m, 1H, ***H*$_5$**), 6.98 (s, 1H, ***H*$_1$**), 6.94 (1H, dd, *J* = 8.5, 2.3 Hz, ***H*$_8$**), 3.81 (s, broad, 2H, N***H*$_2$**). *Data are consistent with literature values*.[2]

2.2. 1H-benzo[e]indole-1,2(3H)-dione

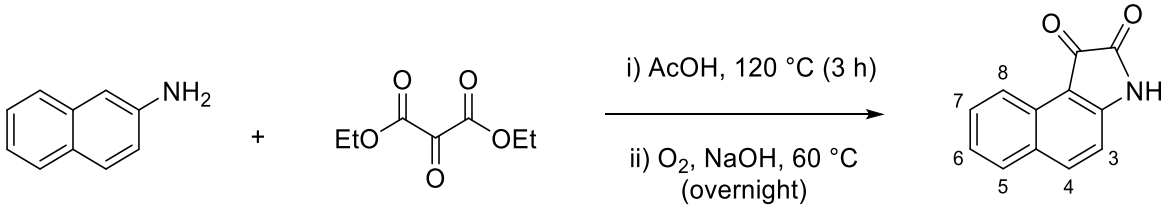

SI 1 **SI 2**

According to a modified procedure of Bruice et *al*,[3] 2-aminonaphthalene **SI 1** (1.60 g, 11.2 mmol, 1.0 eq.) was placed in 90 ml of glacial acetic acid in a round bottom flask fitted with condenser and calcium chloride drying tube. The solution was heated until the complete dissolution of the title compound **SI 1** and diethylmesoxalate (2.04 g, 11.7 mmol, 1.05 eq.) was then added. The solution was stirred at 120 °C for three hours. Afterwards, the solvent was removed in vacuo to deliver a red-brown solid. This solid was then washed with hydrochloric acid (1 M) and suspended in 75 ml of a sodium hydroxide solution (1 M). A slow stream of air was passed through the solution overnight as it was stirred at 60 °C. The orange solution obtained was acidified to pH 3 with hydrochloric acid and the red solid was filtered off after one hour of refrigeration and dried in vacuo. Following the procedure of Karpenko et al.,[4] the residue was finally purified by recrystallization from boiling toluene which gave 1H-benzo[e]indole-1,2(3H)-dione **SI2** as a red solid (1.71 g, 8.66 mmol, 78%). $\mathbf{R_f}$ 0.24 (Cy /EtOAc 3 : 2); **^{1}H NMR (CD_3CN, 300 MHz)** δ 8.89 (1H, s, N***H***), 8.49 (1H, dd, *J* = 8.3, 0.9 Hz, ***H*$_5$**), 8.17 (1H d, *J* = 8.6 Hz ***H*$_4$**), 7.87 (1H, d, *J* = 8.2 Hz, ***H*$_8$**), 7.67 (1H, ddd, *J* = 8.3, 7.0, 1.2 Hz, ***H*$_7$**), 7.44 (1H, ddd, *J* = 8.2, 7.0, 1.2 Hz, ***H*$_6$**), 7.20 (1H, d, *J* = 8.6 Hz, ***H*$_3$**). *Data are consistent with literature values*.[4]

2.3. Methyl 2-amino-1-naphthoate

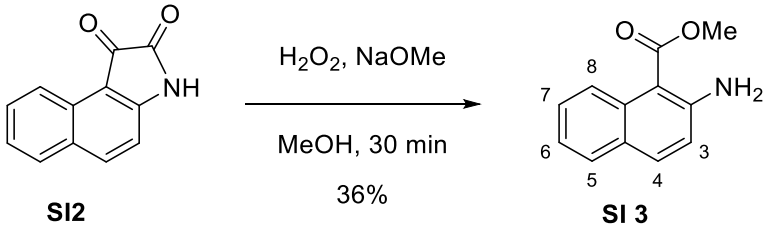

SI2 **SI 3**

According to a modified procedure of *Reissenweber and Mangold*,[5] 1H-benzo[e]indole-1,2(3H)-dione **SI 2** (1.10 g, 5.58 mmol, 1.0 eq.) was suspended in MeOH (0.1 M). Sodium methoxide (30%, 4.75 ml, 3.0 eq.) was then added to the solution. After slow addition of hydrogen peroxide (50%) (227 mg, 6.70 mmol, 1.2 eq.) to the mixture at 0 °C, the initial dark violet solution turned to colourless. The reaction medium was stirred at room temperature for 30 min. The mixture was then acidified by the addition of (1 M, 5 eq.) and stirred at 50 °C for 30 min. The solution was extracted from water with dichloromethane as usual and the solvent was evaporated in vacuo. The residue was finally purified by chromatography on silica gel (60:40 CH_2Cl_2/Cyclohexane) which gave methyl 2-amino-1-naphthoate **SI 3** as a white solid (400 mg, 1.99 mmol, 36%) $\mathbf{R_f}$ 0.28 (CH_2Cl_2/Cyclohexane 3 : 2); **^{1}H NMR ($CDCl_3$, 300 MHz)** δ 8.38 (1H, d, *J* = 8.8 Hz, ***H*$_8$**), 7.55 (2H, m, ***H*$_4$, *H*$_5$**), 7.38 (1H, ddd, *J* = 8.6, 6.9, 1.5 Hz, ***H*$_7$**), 7.15 (1H, ddd, *J* = 8.0, 6.9, 1.0 Hz, ***H*$_6$**), 6.71 (1H, d, *J* = 8.9 Hz, ***H*$_3$**), 5.72 (2H, s, N***H*$_2$**), 3.91 (3H, s, O***Me***).

2.4. (2-aminonaphthalen-1-yl) methanol

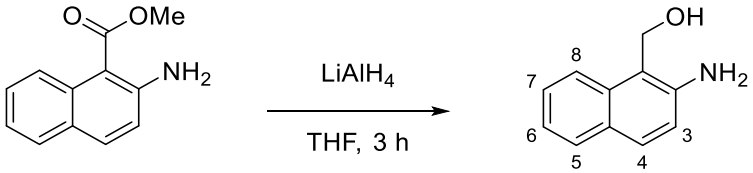

SI 3 **SI 4**

The methyl 2-amino-1-naphthoate (350 mg, 1.74 mmol, 1.0 eq.) **SI 3** was dissolved in dry THF (1M). This solution was then added dropwise to as solution of $LiAlH_4$ (197 mg, 5.22 mmol, 3.0 eq.) in dry THF (0.4 M) at 40 °C. After a 3 h stirring at r.t., EtOAc (25.0 mL) was added, followed by a solution of NaOH 1M (10 mL) until the effervescence stopped. Distilled water (10 mL) was then added to end the quenching. The organic phase was separated and the aqueous phase was finally extracted with EtOAc (3x 25 mL) which gave the title compound **SI 4** as a dark red solid (271 mg, 1.57 mmol, 90%). **^{1}H NMR ($CDCl_3$, 300 MHz)** δ 7.94 (1H, d, *J* = 8.6 Hz, ***H*$_5$**), 7.72 (1H d, *J* = 7.1 Hz ***H*$_8$**), 7.65 (1H, d, *J* = 8.7, Hz, ***H*$_4$**), 7.44 (1H, ddd, *J* = 8.4, 6.9, 1.4 Hz, ***H*$_6$**), 7.25 (1H, ddd, *J* = 7.9, 6.8, 0.9 Hz, ***H*$_7$**), 6.96 (1H, d, *J* = 8.7 Hz, ***H*$_3$**), 5.10 (2 H, s, C***H*$_2$**OH).

2.5. 5-nitro-1,10-phenanthroline

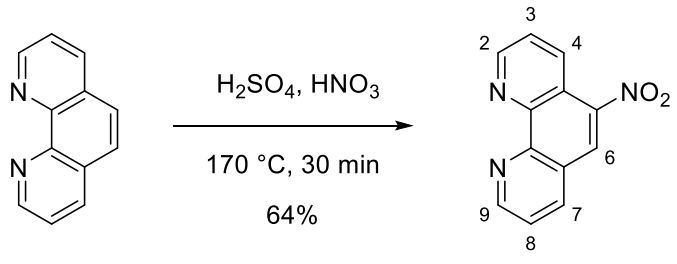

SI 5

Firstly, 1,10-phenanthroline (10.0 g, 55.5 mmol) was dissolved in a mixture containing 120 mL H_2SO_4 (18 M) and 80 mL HNO_3 (64%). The solution was then stirred at 170°C for 30 min. After cooling down to room temperature, the medium was diluted with 400 g of ice. The acidic solution was then neutralized by addition of NaOH (30 %). The so formed yellow precipitate was filtered and washed with water which gave the title compound **SI 5** as a yellow solid (7.63 g, 33.8 mmol, 61%). $\mathbf{R_f}$ 0.5 (CH_2Cl_2 / MeOH 95:5); **^{1}H NMR (CD_3OD, 300 MHz)** δ 9.16 (1H, dd, *J* = 4.4, 1.7 Hz, ***H*$_9$**), 9.12 (1H, dd, *J* = 4.3, 1.6 Hz, ***H*$_2$**), 8.89 (1H dd, *J* = 8.6, 1.6 Hz, ***H*$_7$**), 8.73 (1H, s, ***H*$_6$**), 8.57 (dd, *J* = 8.2, 1.7 Hz, ***H*$_4$**), 7.89-7.80 (2H, m, ***H*$_{3\text{-}8}$**). *NMR data are consistent with literature values.*[6]

2.6. 5-amino-1,10-phenanthroline

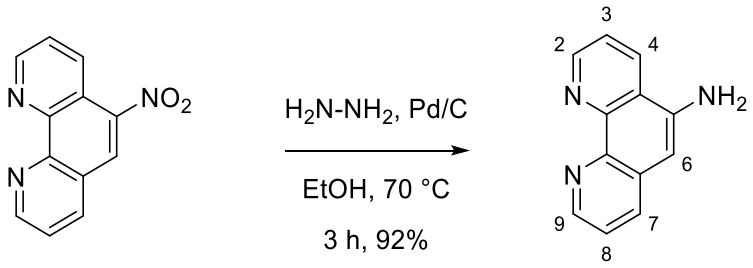

SI 5 **SI 6**

Pd/C catalyst (10%, 110 mg) and 5-nitro-1,10-phenanthroline **SI 5** (500 mg, 2.22 mmol, 1.0 eq.) were dissolved in ethanol (15 ml). A solution of hydrazine (64 %, 355 mg, 11.1 mmol, 5.0 eq.) diluted in 15 ml of ethanol was then added dropwise to the medium over 10 minutes. Afterwards, the mixture was stirred at 70 °C for 3 h. After cooling down to room temperature, the solution was filtered on celite and concentrated to 15 ml under vacuum. Water was then added to the mixture and the so formed yellow precipitate was filtered and dried under vacuum. 5-amino-1,10-phenanthrolin **SI6** was delivered as a yellow solid (399 mg, 2.04 mmol, 92%). $\mathbf{R_f}$ 0.32 (CH_2Cl_2 / MeOH 95:5); **^{1}H NMR (CD_3OD, 300 MHz)** δ 9.06 (1H, dd, *J* = 4.3, 1.6 Hz, ***H*$_2$**), 8.73 (1H, dd, *J* = 4.4, 1.6 Hz, ***H*$_4$**), 8.63 (1H dd, *J* = 8.4, 1.6 Hz, ***H*$_9$**), 8.08 (1H, dd, *J* =8.2, 1.6 Hz, ***H*$_7$**), 7.74 (dd, *J* = 8.4, 4.4 Hz, ***H*$_8$**), 7.55 (1H, dd, *J* = 8.2, 4.4 Hz, ***H*$_3$**), 6.99 (1H, s, ***H*$_6$**). *NMR data are consistent with literature values.*[6]

2.7. Naphtho[2,1-b]pyrido[3,2-f][1,7]phenanthroline (NAPP)

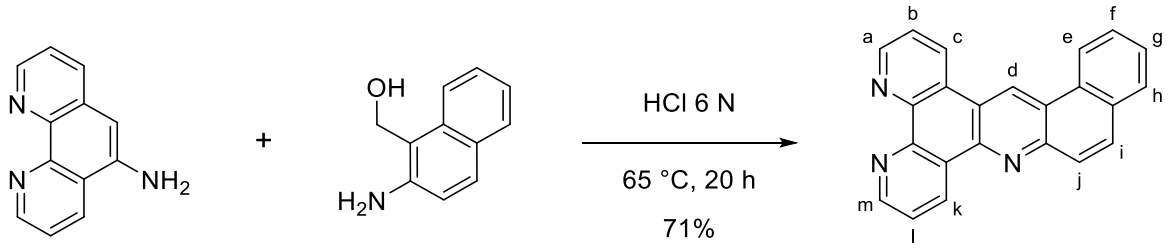

SI 6 **SI 4** **NAPP**

According to a procedure of Deraedt and Elias,[7] 1,10-phenanthrolin-5-amine **SI 6** (187 mg, 0.956 mmol, 1.0 eq.) and (2-aminonaphthalen-1-yl)methanol **SI 4** (164 mg, 0.959 mmol, 1.0 eq.) were suspended in 6N HCl (7 ml). The solution was stirred for 20 h at 65 °C. Then the mixture was cooled down to room temperature and the acidity was quenched by addition of aqueous ammonia until reaching pH 9. The so formed orange precipitate was filtered and washed with water. The solid was finally purified by chromatography on neutral alumina (100% CH_2Cl_2 to 90:10 CH_2Cl_2/MeOH) which gave naphtho[2,1-b]pyrido[3,2-f][1,7]phenanthroline **NAPP** as a beige solid (224 mg, 0.679 mmol, 71%) An analytic sample was obtained by recrystallizing the product from boiling methanol. **^{1}H NMR**

(CD$_3$CN, 500 MHz) δ 10.09 (1H, s, ***H$_d$***), 9.61 (1H, dd, $J_{a\text{-}b}$ = 8.1, $J_{a\text{-}c}$ = 1.8 Hz, ***H$_a$***), 9.29 (1H, dd, $J_{k\text{-}l}$ = 8.3, $J_{k\text{-}m}$ = 1.4 Hz, ***H$_k$***), 9.14 (1H, dd, $J_{c\text{-}b}$ = 4.3, $J_{c\text{-}a}$ = 1.8 Hz, ***H$_c$***), 9.10 (1H, dd, $J_{m\text{-}l}$ = 4.3, $J_{m\text{-}k}$ = 1.5 Hz ***H$_m$***), 9.04 (1H, d, $J_{e\text{-}f}$ = 8.2 Hz, ***H$_e$***), 8.12 (1 H, d, $J_{j\text{-}i}$ = 9.1 Hz, ***H$_i$***), 8.05 (1 H, d, $J_{j\text{-}i}$ = 9.2 Hz, ***H$_j$***), 8.03 (1 H, d, $J_{h\text{-}g}$ = 7.3 Hz, ***H$_h$***), 7.85-7.79 (2 H, m, ***H$_{f,g}$***), 7.79-7.74 (2 H, m, ***H$_{l,b}$***); **HRMS-ESI** calculated for $C_{23}H_{14}N_3$ ([M+H]$^+$) : *m/z* 332.11822, found: *m/z* 332.11816.

2.8. [Ru(bpy)2napp]2+

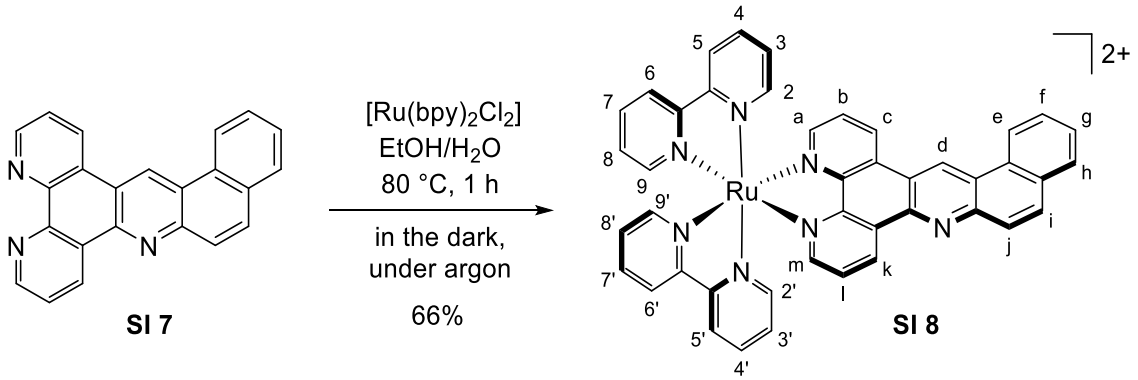

The dichloro precursor [Ru(bpy)$_2$Cl$_2$] (20 mg, 0.041 mmol, 1.0 eq) and NAPP (20 mg, 0.061 mmol, 1.5 eq) were mixed in a solution of absolute ethanol/water (50/50, 5 mL). The reaction medium was then stirred at 80 °C until the precurssor was consumed as monitored by TLC (3 h). Afterwards, ethanol was evaporated and addition of small portions of NH_4PF_6 yielded to the formation of an orange precipitate. After centrifugation, the solid was washed several times with water and was then dried in vacuo. The so formed orange-red crude was finally purified by chromatography on silica gel (CH_3CN/H_2O/ KNO_{3sat} 10:1:1/2) which gave **[Ru(bpy)2napp]2+** as an orange solid (28 mg, 0.027 mmol, 66%). The counter-anion exchange from PF_6 to Cl was performed by adding small portions of NBu_4Cl to a solution of the complex in acetone. **R$_f$** 0.35 (CH_3CN/H_2O/ KNO_{3sat} 10:1:1/2); **^{1}H NMR (CD$_3$CN, 500 MHz)** δ (ppm), 10.47 (1H, s, ***H$_d$***), 9.81 (1H, d, $J_{a\text{-}b}$ = 8.2, $J_{a\text{-}c}$ = 1.2 Hz, ***H$_a$***), 9.59 (1H, dd, $J_{c\text{-}b}$ = 8.2, $J_{c\text{-}a}$ = 1.2 Hz, ***H$_c$***), 9.24 (1H, d, $J_{m\text{-}l}$ = 8.2 Hz, ***H$_k$***), 8.53 (4H, m, ***H$_5$, H$_{5'}$, H$_6$, H$_{6'}$***), 8.34 (1H, d, $J_{i\text{-}j}$ = 9.1 Hz, ***H$_i$***), 8.25 (1H, d, $J_{j\text{-}i}$ = 9.1 Hz, ***H$_j$***), 8.16 (2H, m, ***H$_4$, H$_{4'}$***), 8.12 (3H, m, ***H$_e$, H$_f$, H$_g$***), 8.01 (2H, m, ***H$_7$, H$_{7'}$***), 7.95 (1H, m, ***H$_l$***), 7.91-7.84 (5H, m, ***H$_b$, H$_2$, H$_{2'}$, H$_m$, H$_h$***), 7.73 (1H, d, $J_{9\text{-}8}$ = 5.4 Hz, ***H$_9$***), 7.69 (1H, d, $J_{9'\text{-}8'}$ = 5.6 Hz, ***H$_{9'}$***), 7.49-7.44 (2H, m, ***H$_3$, H$_{3'}$***), 7.28-7.21 (m, 2H, ***H$_8$, H$_{8'}$***); **HRMS-ESI** calculated for [$C_{43}H_{29}N_7F_6PRu$]$^+$: *m/z* 890.11728, found: *m/z* 890.11700 and for [$C_{43}H_{29}N_7Ru$]$^{2+}$: *m/z* 372.57617, found: *m/z* 372.57640. The product yielding was confirmed by elemental composition analysis and X-ray crystallography.

3. NMR spectra

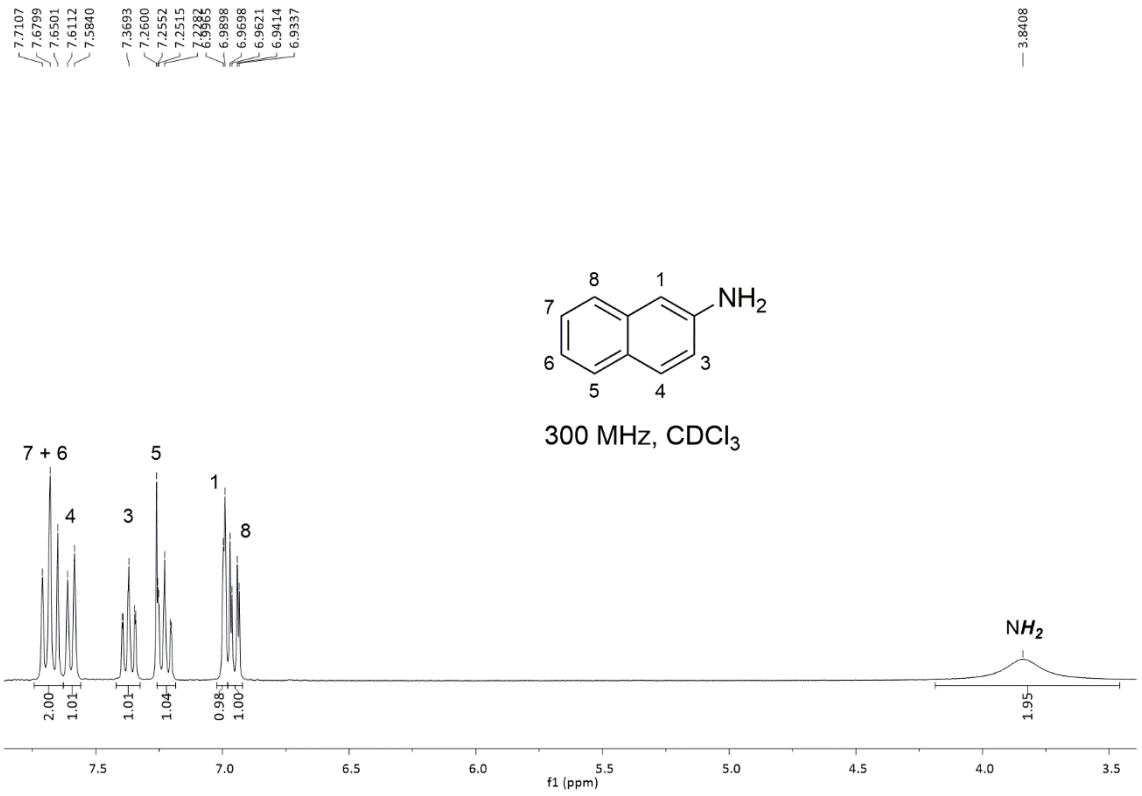

Figure S 3 ^{1}H NMR spectra of **SI 1** (300 MHz, CDCl3).

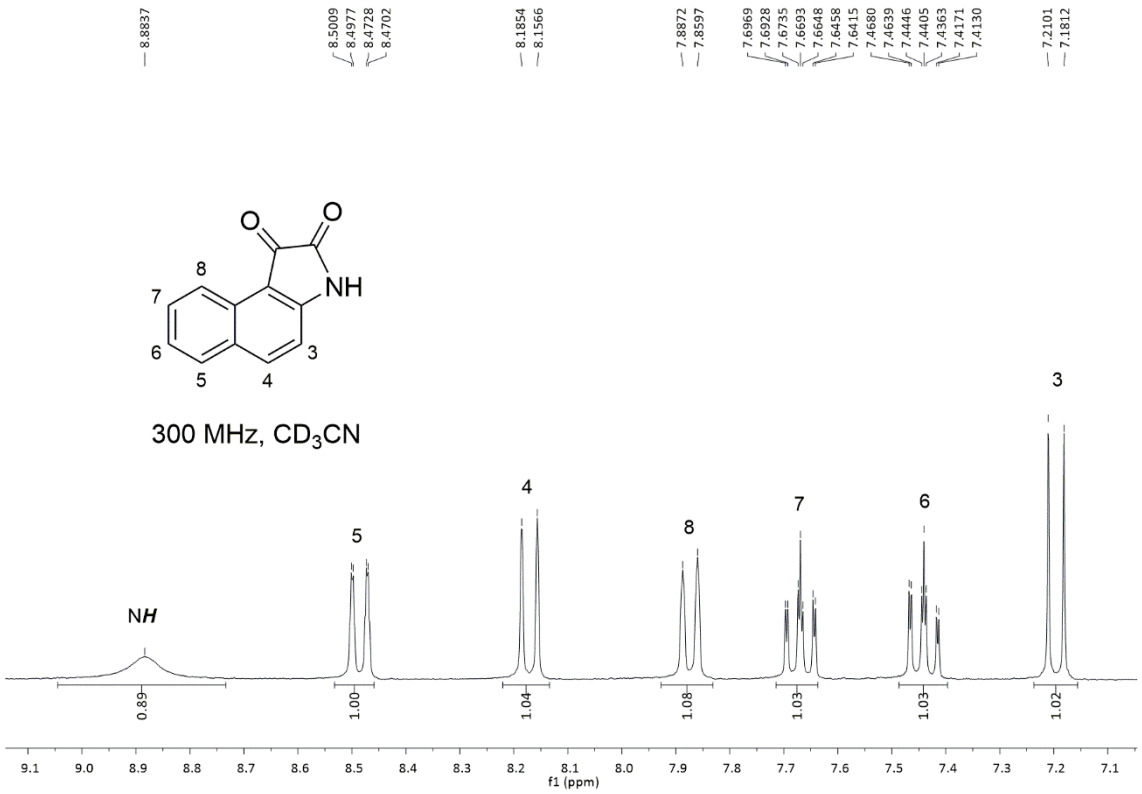

Figure S 4 ^{1}H NMR spectra of **SI 2** (300 MHz, CD_3CN).

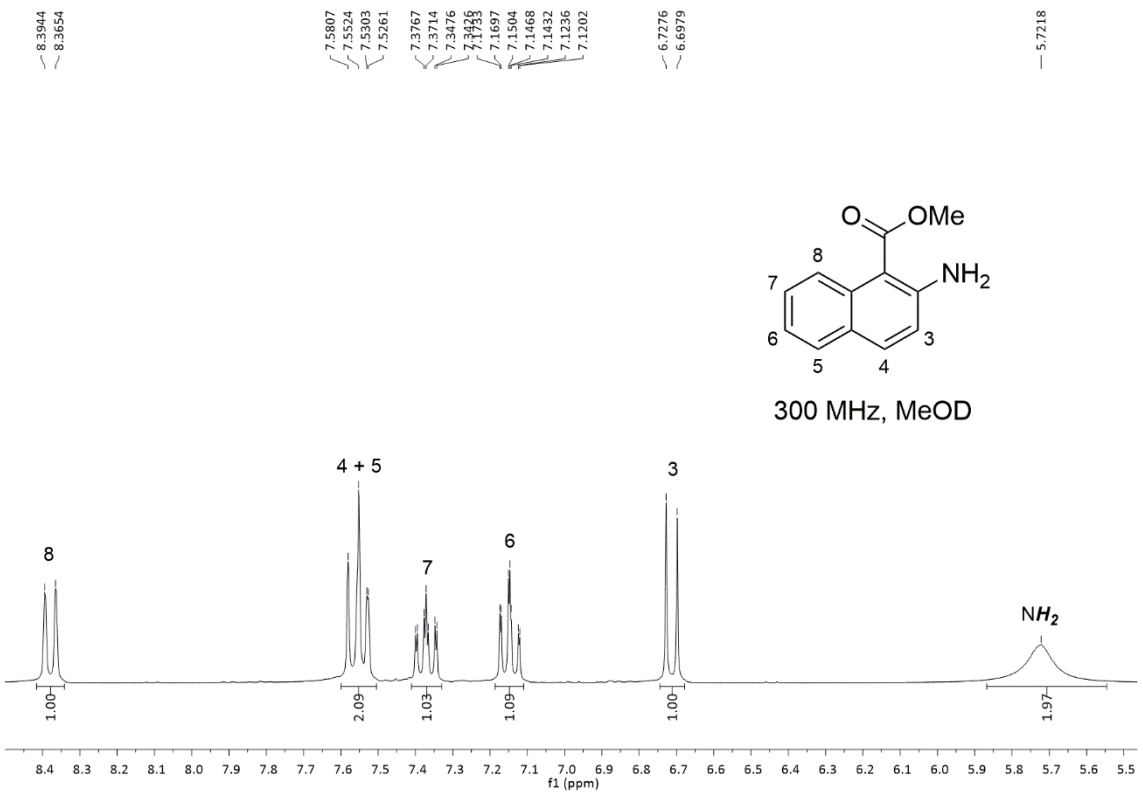

Figure S 5 ^{1}H NMR spectra of **SI 3** (300 MHz, MeOD).

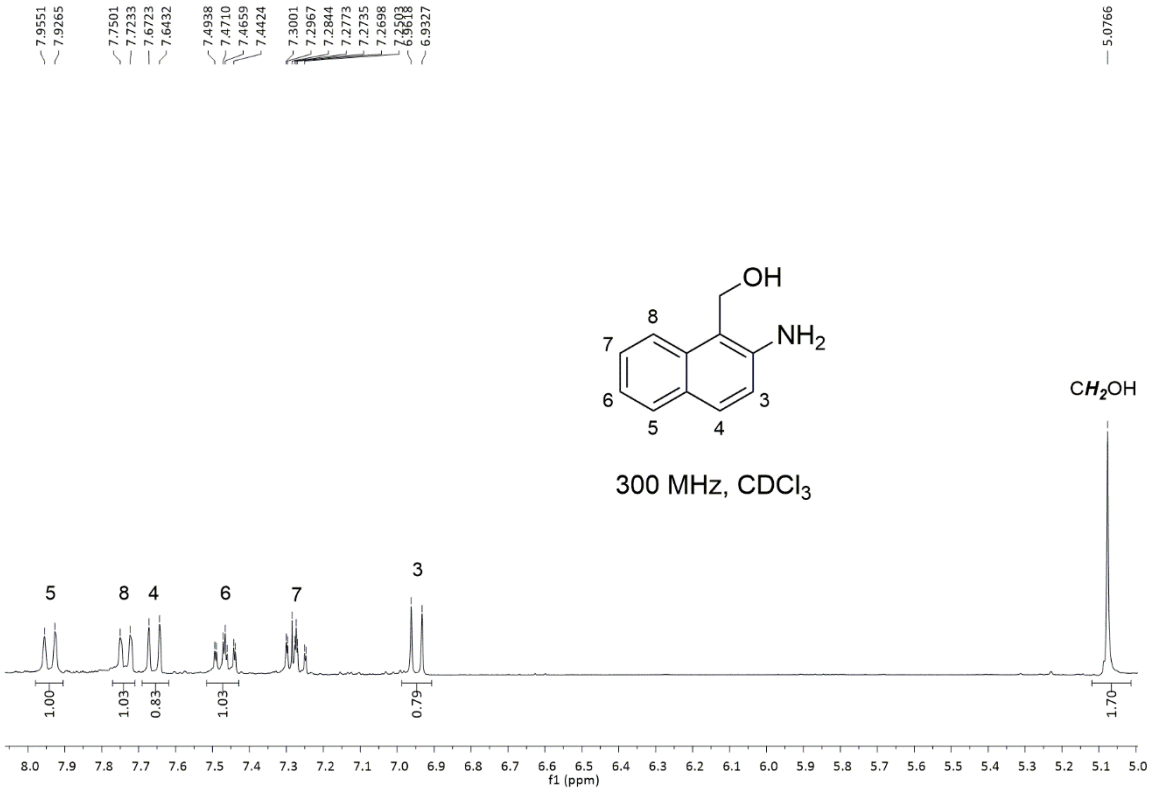

Figure S 6 ^{1}H NMR spectra of **SI 4** (300 MHz, CDCl3).

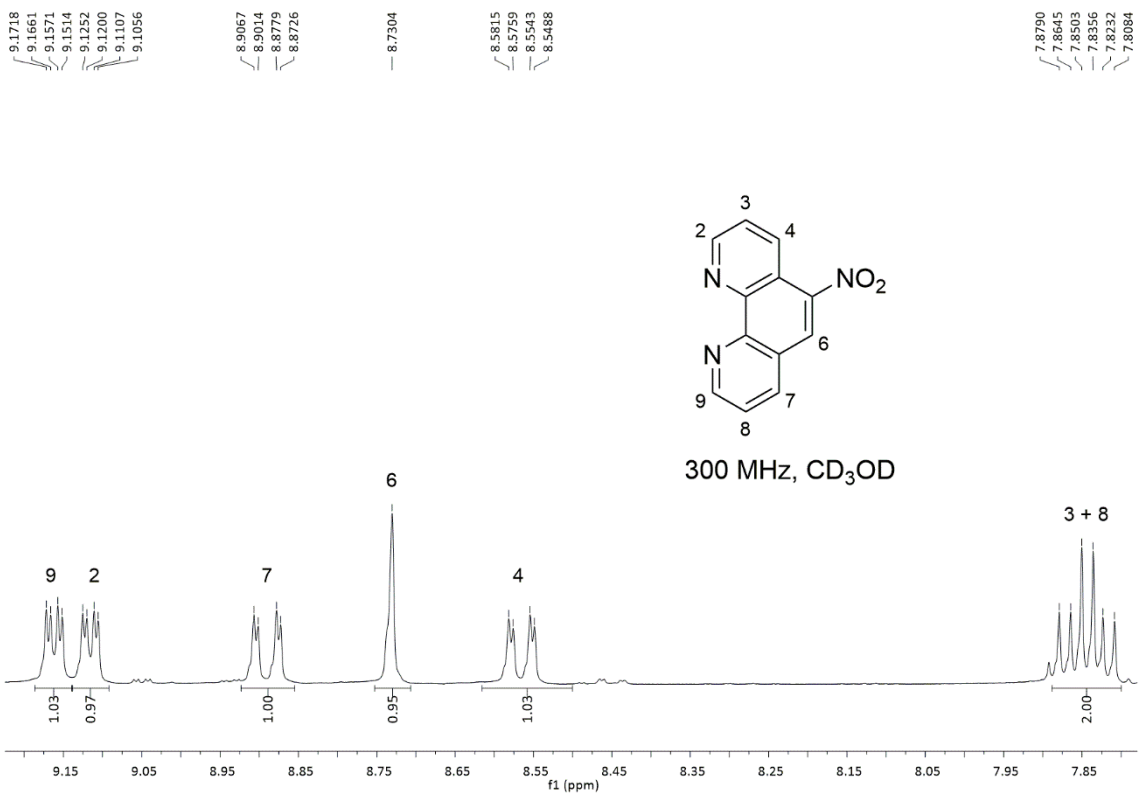

Figure S 7 [1]H NMR spectra of **SI 5** (300 MHz, MeOD).

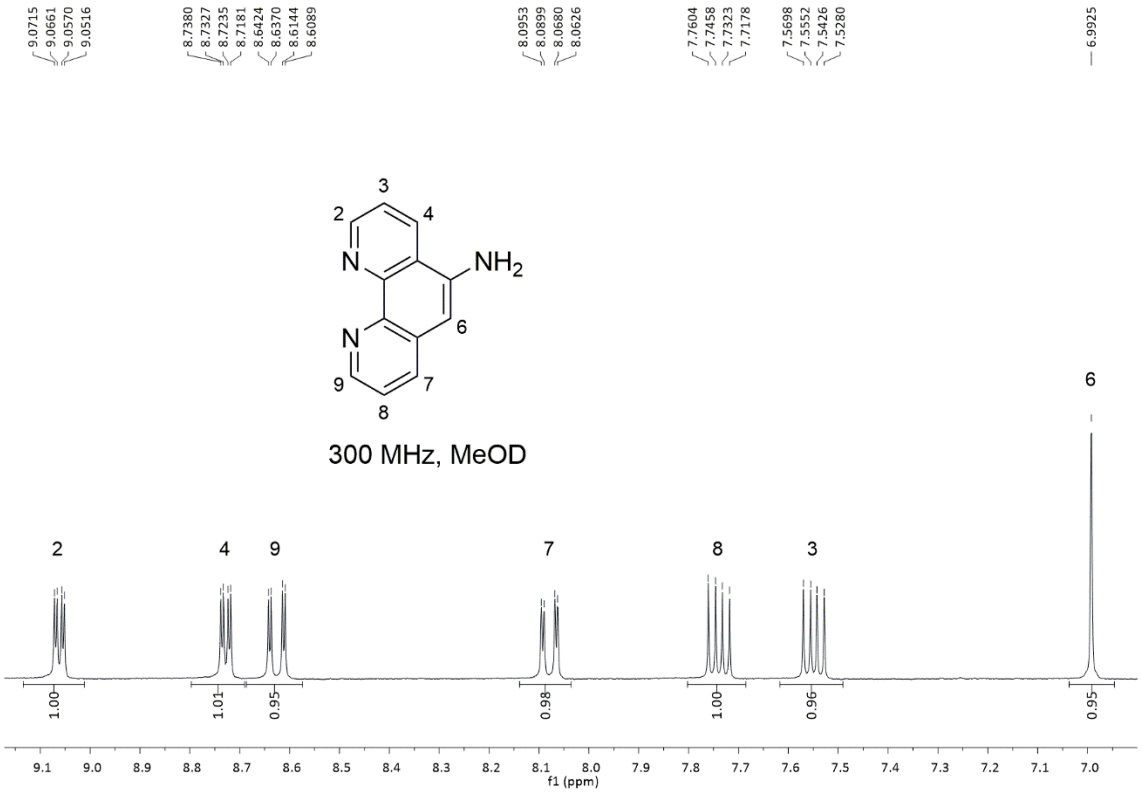

Figure S 8 [1]H NMR spectra of **SI 6** (300 MHz, MeOD).

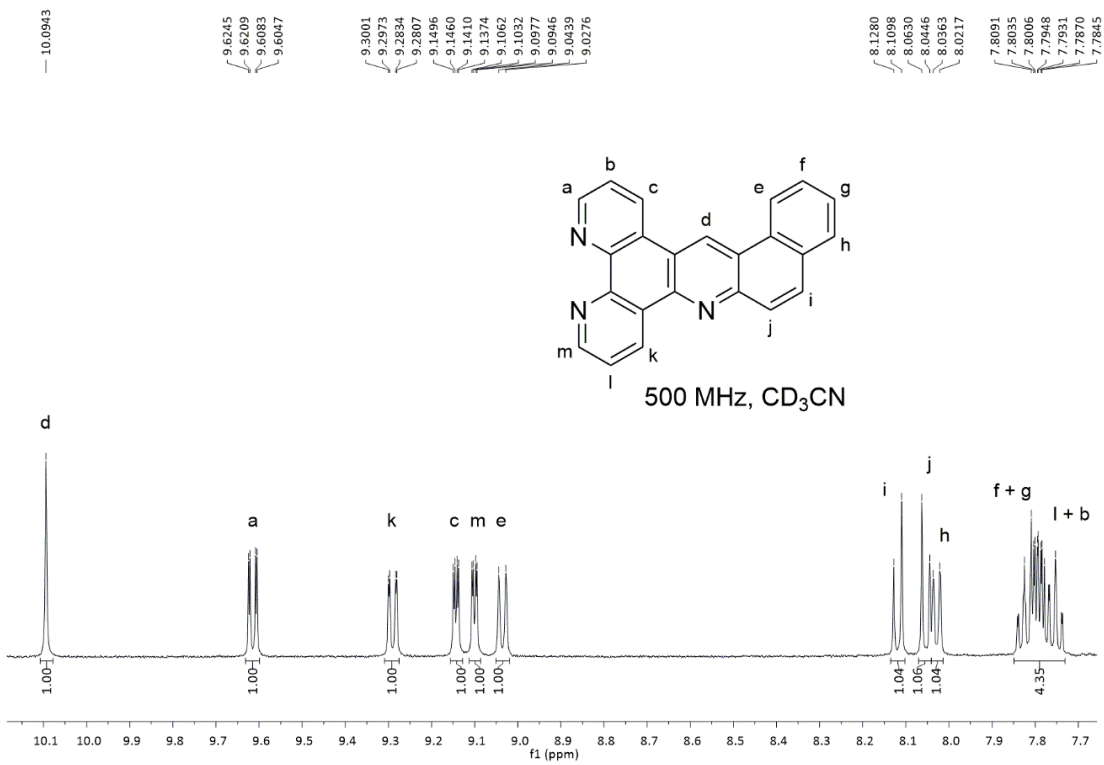

Figure S 9 ^{1}H NMR spectra of **NAPP** (500 MHz, CD_3CN).

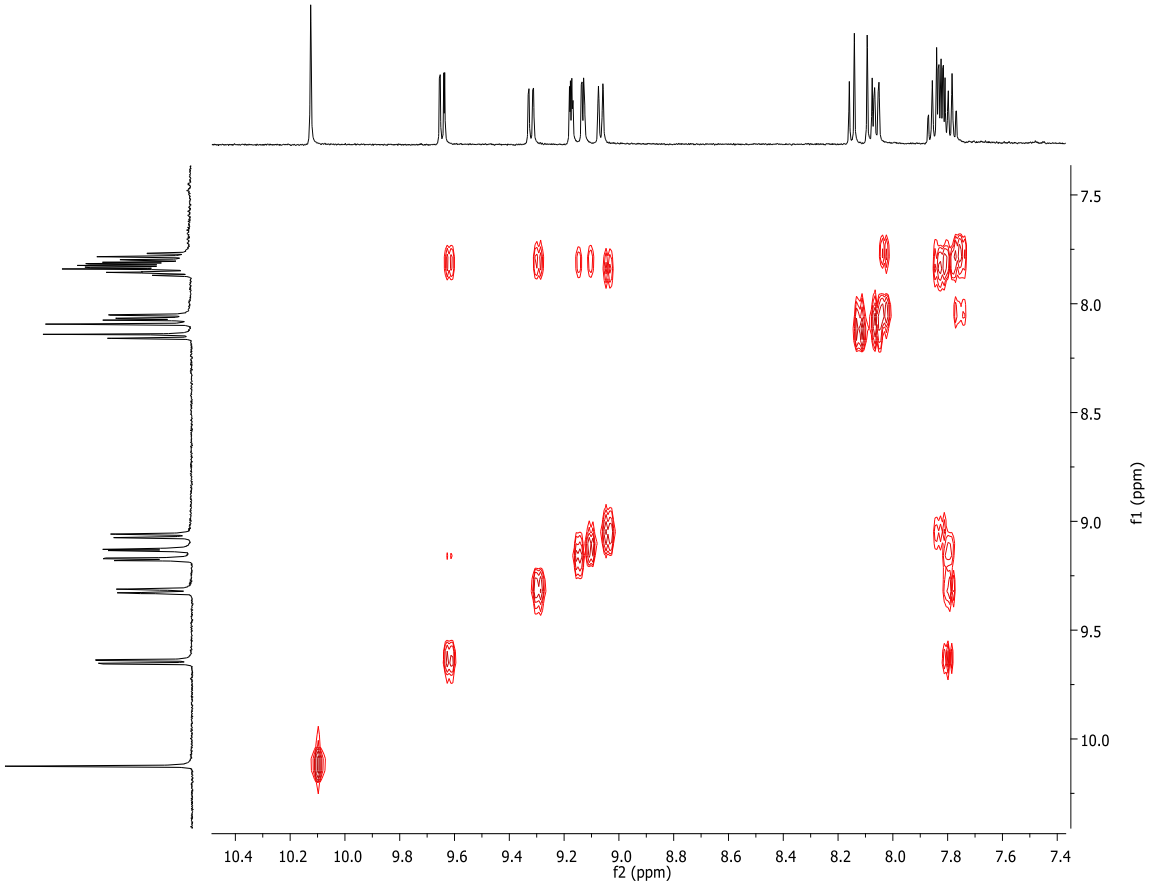

Figure S 10 COSY ^{1}H^{1}H NMR spectra of **NAPP** (500 MHz, CD3CN).

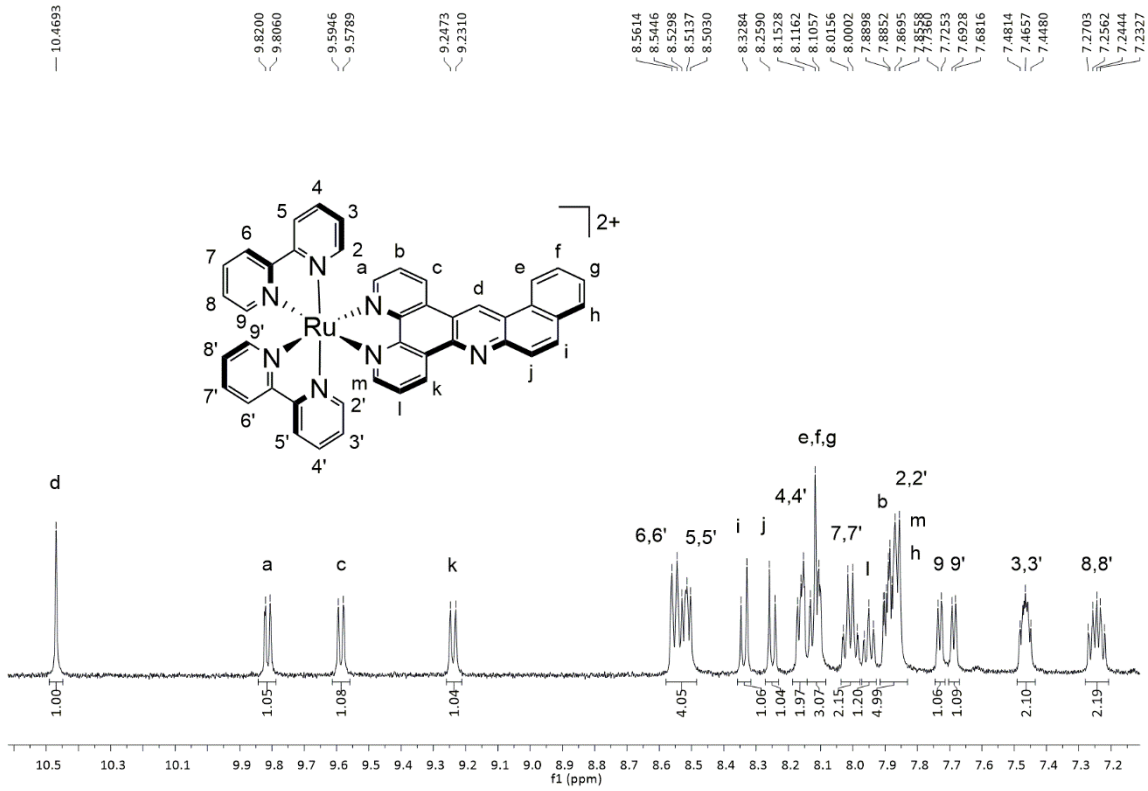

Figure S 11 ^{1}H NMR spectra of **[RU(BPY)2NAPP]2+** (500 MHz, CD_3CN).

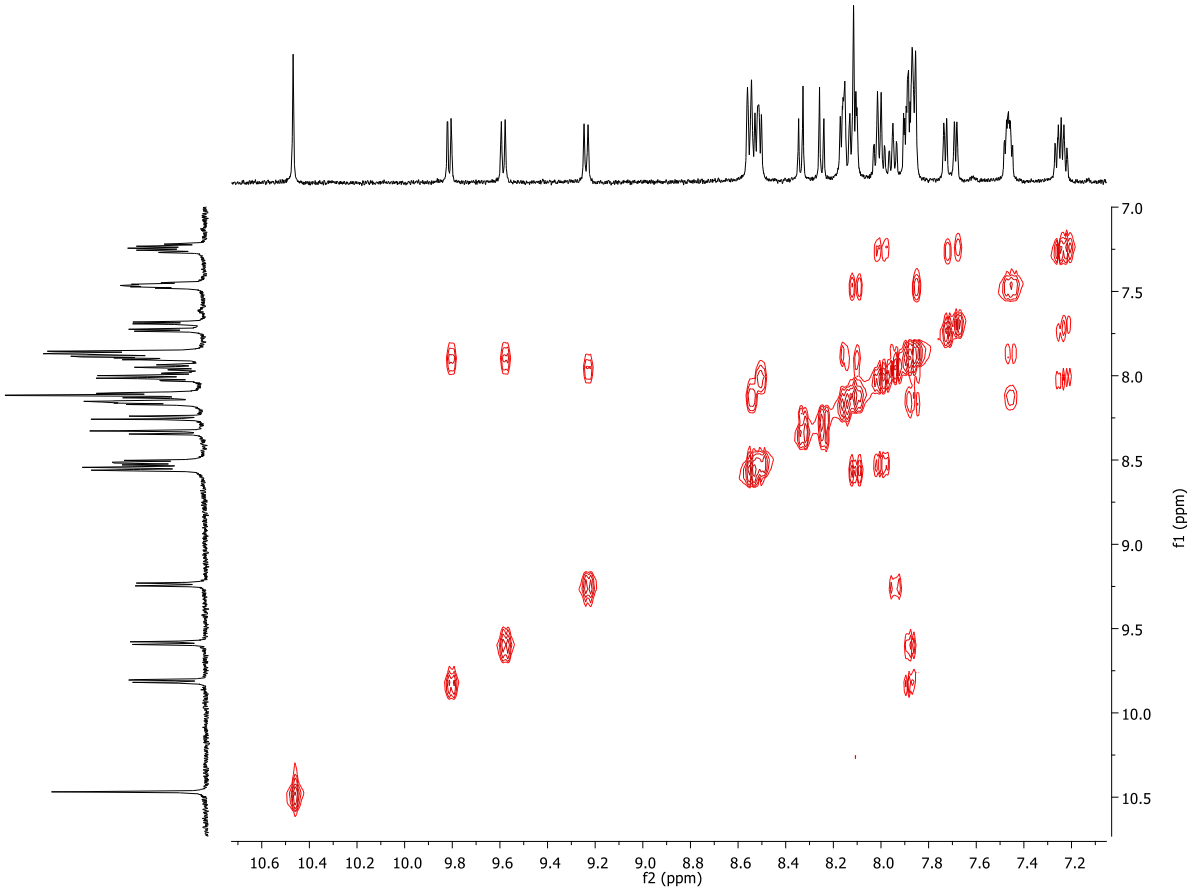

Figure S 12 COSY ^{1}H^{1}H NMR spectra of **[RU(BPY)2NAPP]2+** (500 MHz, CD3CN).

4. HRMS data and elemental composition

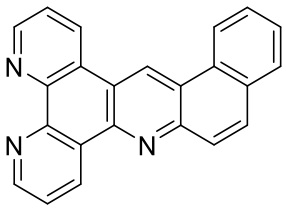

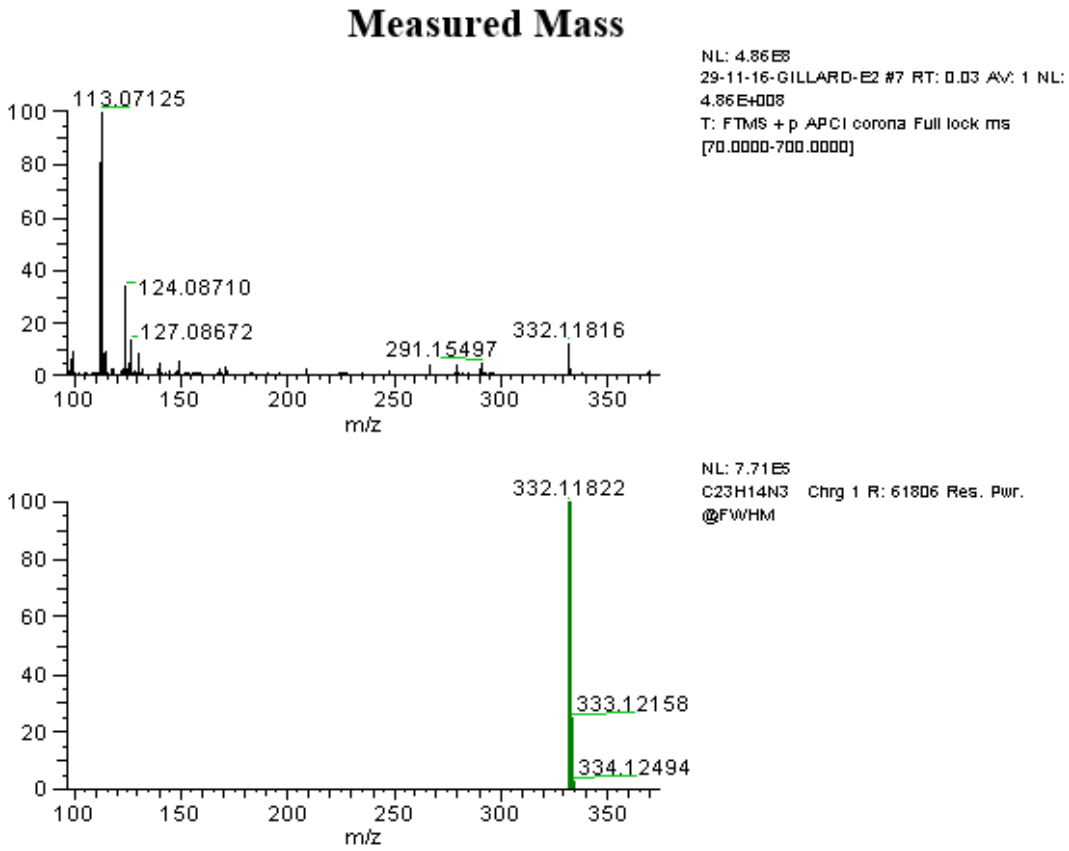

Elemental Composition Results

m/z	Formula	Score	Delta ppm	OriginalFormula	Theo. Mass
332.11816	$C_{23}H_{14}N_3$	100.00	-0.18	C23H14N3	332.11822

Figure S 13 HRMS data for **NAPP**. *Peak of reserpine as internal standard.

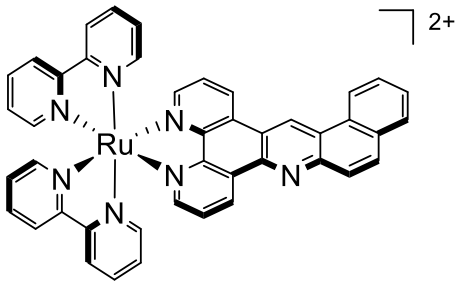

Measured Mass

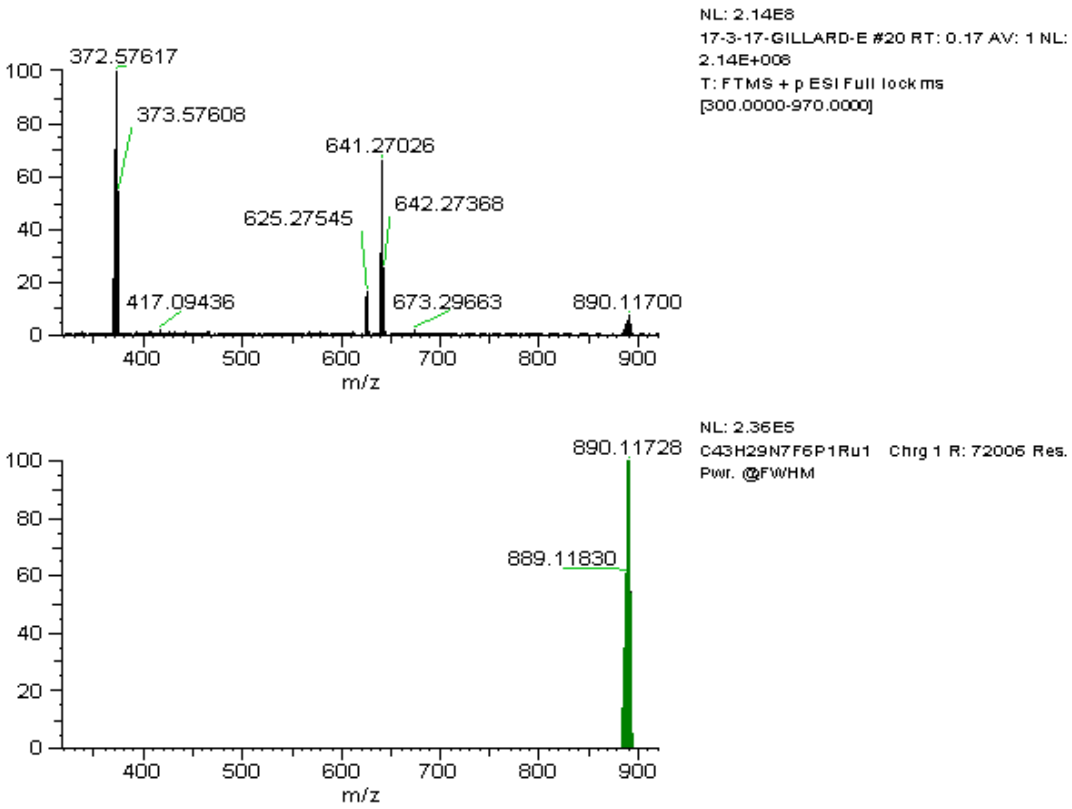

Elemental Composition Results

m/z	Formula	Score	Delta ppm	OriginalFormula	Theo. Mass
884.11938	$C_{43}H_{29}N_7F_6P^{96}Ru$	77.05	-0.33	C43H29N7F6P[96]Ru	884.11967

Figure S 14 HRMS data for **[RU(BPY)2NAPP]2+**. *Peak of reserpine as internal standard.

5. X-ray crystallography of $[Ru(bpy)_2napp]^{2+}$

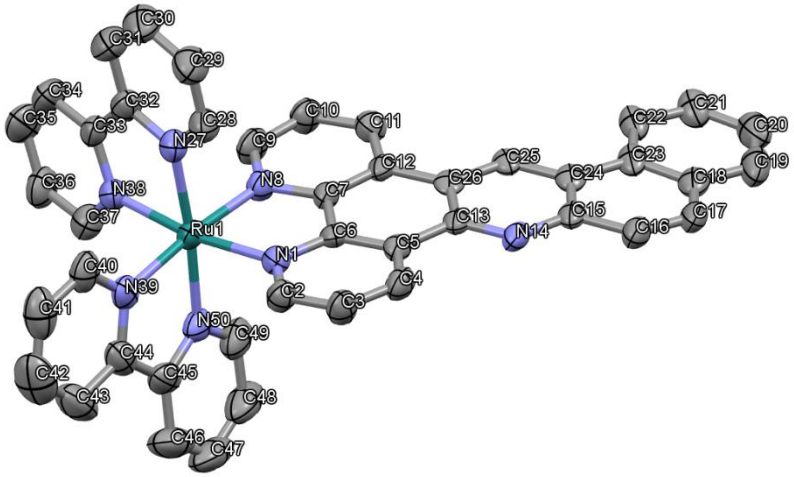

Figure S 15 X-ray crystallography of **$[Ru(bpy)_2napp]^{2+}$** with atom numbering. Displacement ellipsoids of non-hydrogen atoms are drawn at the 50 % probability level. Hydrogen atoms were omitted for clarity.

Diffraction data were recorded on a MAR345 detector using monochromated Mo Kα radiation (λ = 0.71073 Å) (Xenocs Fox3D mirror) produced by a Rigaku UltraX 18 generator.

A plate like orange-red crystal was mounted on a nylon loop and flash-frozen at 150K in a gaseous N_2 stream prior to the measurement. A total of 135+50 images $\Delta\phi$=2° were taken at two different orientations of the crystal.

The structure was solved by SHELXT (Sheldrick, 2015) and then refined on $|F^2|$ using SHELXL-2014. Non-hydrogen atoms were anisotropically refined and hydrogen atoms were placed in calculated positions and refined in riding mode with isotropic temperature factors fixed at 1.2 times U(eq) of the parent atoms (1.5 times for methyl groups).

The **$[Ru(bpy)_2napp]^{2+}$** structure crystallizes in the triclinic space group *P-1* with two molecules in the asymmetric unit (Z' = 2) giving a total of 4 molecules in the unit cell. The overall geometry around the Ru-atom is found to be octahedral and the positive charge (+II) is counterbalanced by 2 time 2 PF_6 anions, of which two are found to be disordered over two sites.

The structure contains large voids, a total of 273.41 $Å^3$, 6.2% of the unit cell volume, which was treated by the squeeze algorithm (Platon, 2008). Because of the observed disorder a smaller than default probe radius was used (0.8 opposed to 1.2Å), for which Squeeze found 167 electrons, which were subsequently added to the void as a smeared-out electron density. These cavities probably contain (partially occupied) solvent molecules from the crystallization medium (Acetonitrile/ether).

No hydrogen bonding is observed and the packing is stabilized by parallel displaced π-π stacking; The PF_6 anions are arranged in-between complexes, adjacent to the cavities. Given the disordered nature of some PF_6 anions, no strong interactions with the ligands will be present.

Crystal data and structure refinement for **$[Ru(bpy)_2napp]^{2+}$**

Identification code	**$[Ru(bpy)_2napp]^{2+}$**
Empirical formula	$C_{43}\ H_{29}\ F_{12}\ N_7\ P_2\ Ru$
Formula weight	1034.74
Temperature	150(2) K

Wavelength	0.71073 Å
Crystal system	Triclinic
Space group	P-1
Unit cell dimensions	a = 13.3187(7) Å
	b = 17.8256(13) Å
	c = 19.9502(11) Å
	α= 108.363(6)°.
	β= 93.931(5)°.
	γ = 97.687(5)°.
Volume	4423.9(5) Å3
Z	4
Density (calculated)	1.554 Mg/m3
Absorption coefficient	0.518 mm-1
F(000)	2072
Crystal size	0.360 x 0.060 x 0.020 mm3
Theta range for data collection	3.074 to 25.242°.
Reflections collected	52163
Independent reflections	15778 [$R_{(int)}$ = 0.0824]
Completeness to theta = 25.242°	98.6 %
Absorption correction	Semi-empirical from equivalents
Max. and min. transmission	1.00000 and 0.54816
Refinement method	Full-matrix least-squares on F2
Data / restraints / parameters	15778 / 378 / 1299
Goodness-of-fit on F2	1.089
Final R indices [I>2sigma(I)]	R_1 = 0.0889, wR2 = 0.1817
R indices (all data)	R_1 = 0.1233, wR2 = 0.1989
Largest diff. peak and hole	1.613 and -0.578 e.Å-3

6. Cyclic voltammograms of $[Ru(bpy)_2napp]^{2+}$

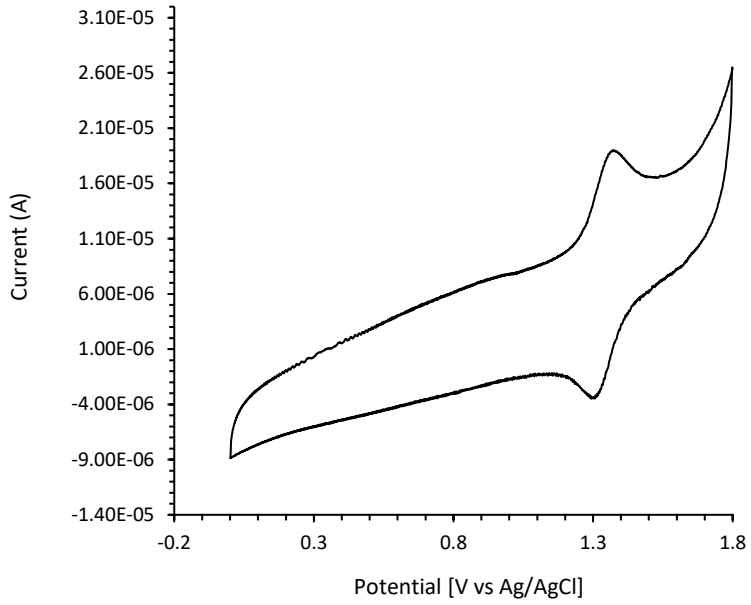

Figure S 16 Cyclic voltammogram of **$[Ru(bpy)_2napp]^{2+}$** oxidation recorded in dry acetonitrile under argon, with a sweep rate of 0.3 V/s, at room temperature. The concentration of the complex is 8.10^{-4} mol/L, with 0.1 mol/L tetrabutylammonium perchlorate as supporting electrolyte.

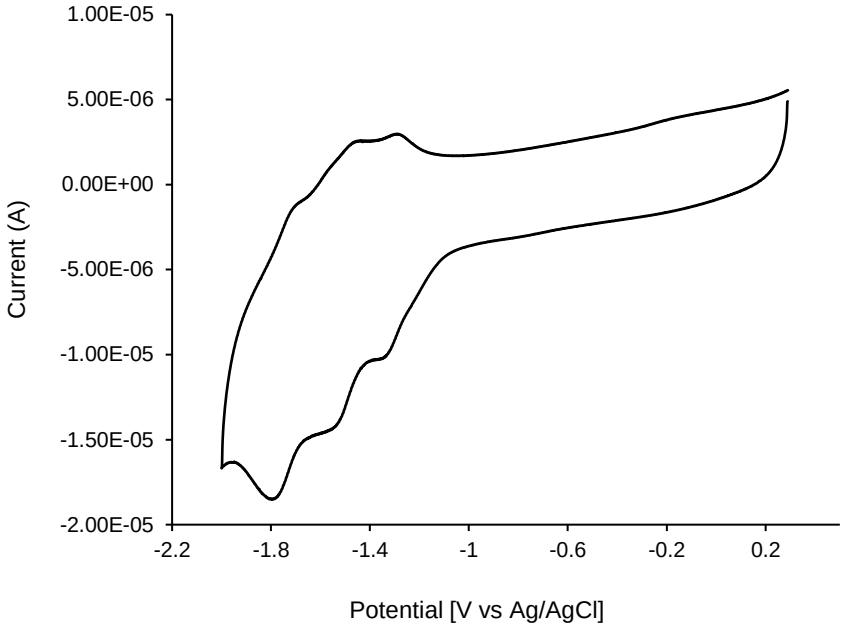

Figure S 17 Cyclic voltammogram of **$[Ru(bpy)_2napp]^{2+}$** reduction recorded in dry acetonitrile under argon, with a sweep rate of 0.3 V/s, at room temperature. The concentration of the complex is 8.10^{-4} mol/L, with 0.1 mol/L tetrabutylammonium perchlorate as supporting electrolyte.

7. Computational data

Gaussian 16, Revision A03 was used for all theoretical calculations discussed herein.[1] The molecular structure of the metal complex was fully optimized with CPCM acetonitrile solvation model in absence of constraints at Density Functional Theory (DFT) level. In particular, the hybrid PBE0 functional,[2] casting 25% of HF exchange in the PBE functional was applied.[3] A double zeta valence basis set was used for all atoms but Ru ones which were described by the Los Alamos pseudo potential and corresponding basis set.[4] No imaginary frequencies were obtained when frequency calculations on optimized geometries were performed. GaussView 6.0.16, Chemissian 4.44 softwares were used for data analysis, visualization and surface plots.[5]

Theoretical calculations

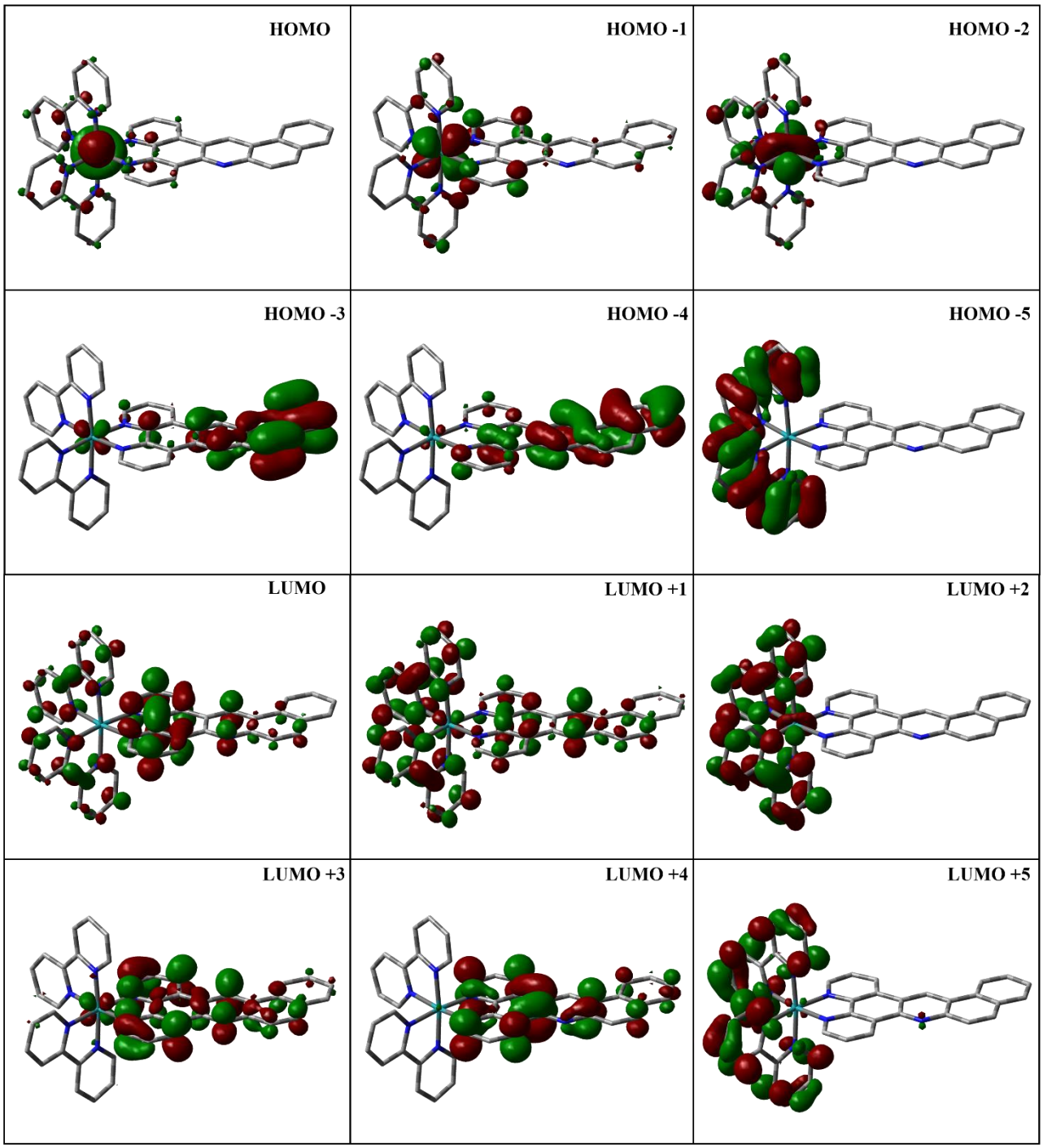

Figure S 18 Representation of the orbitals LUMO+4 to HOMO-4 with the contributions of the different fragments of **[Ru(bpy)$_2$napp]$^{2+}$** modelled in water.

Table MO composition of **[Ru(bpy)$_2$napp]$^{2+}$** in water.

MO	Energy (eV)	Composition		
		Ru	2,2'-bpy	**napp**
LUMO+5	-1.722	**1**	95	4
LUMO+4	-2.329	1	2	98
LUMO+3	-2.429	4	7	89
LUMO+2	-2.498	6	92	2
LUMO+1	-2.549	3	59	39
LUMO	**-2.654**	**0**	**34**	**66**
HOMO	**-6.370**	**82**	**12**	**6**
HOMO-1	-6.509	68	11	20
HOMO-2	-6.548	75	21	4
HOMO-3	-6.818	5	1	94
HOMO-4	-7.107	1	0	98
HOMO-5	-7.767	0	96	3

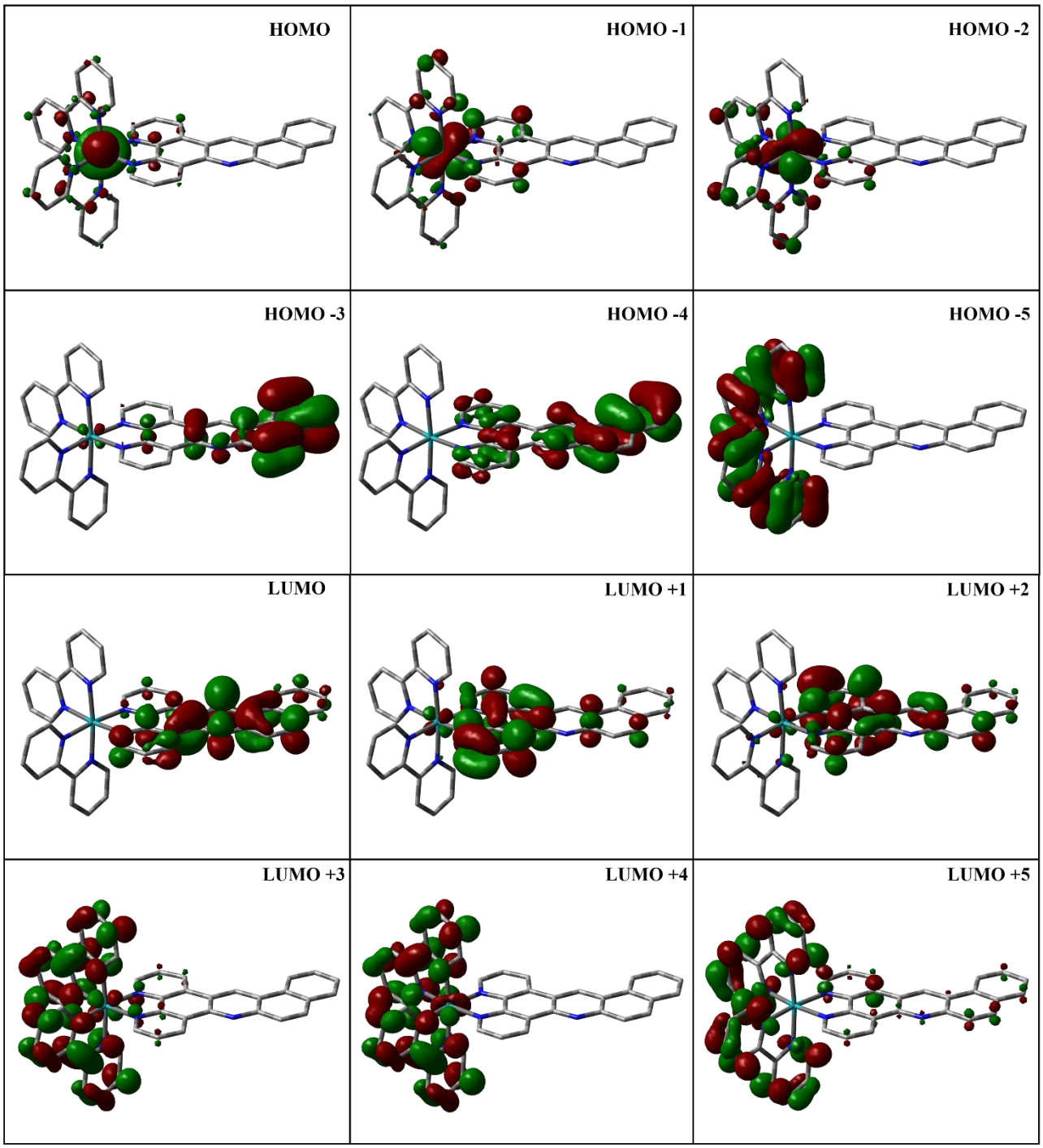

Figure S 19 Representation of the orbitals LUMO+4 to HOMO-4 with the contributions of the different fragments of **$[Ru(bpy)_2napp\text{-}H]^{2+}$** modelled in water.

Table MO composition of **[Ru(bpy)$_2$napp-H]$^{2+}$** in water.

MO	Energy (eV)	Composition		
		Ru	2,2'-bpy	**napp**
LUMO+5	-1.820	**1**	84	15
LUMO+4	-2.564	6	93	1
LUMO+3	-2.626	4	7	89
LUMO+2	-2.819	2	92	6
LUMO+1	-2.914	2	4	94
LUMO	**-3.635**	**0**	**0**	**100**
HOMO	**-6.525**	**82**	**13**	**6**
HOMO-1	-6.692	73	13	14
HOMO-2	-6.701	75	20	5
HOMO-3	-7.367	2	1	98
HOMO-4	-7.731	0	1	99
HOMO-5	-7.829	0	99	1

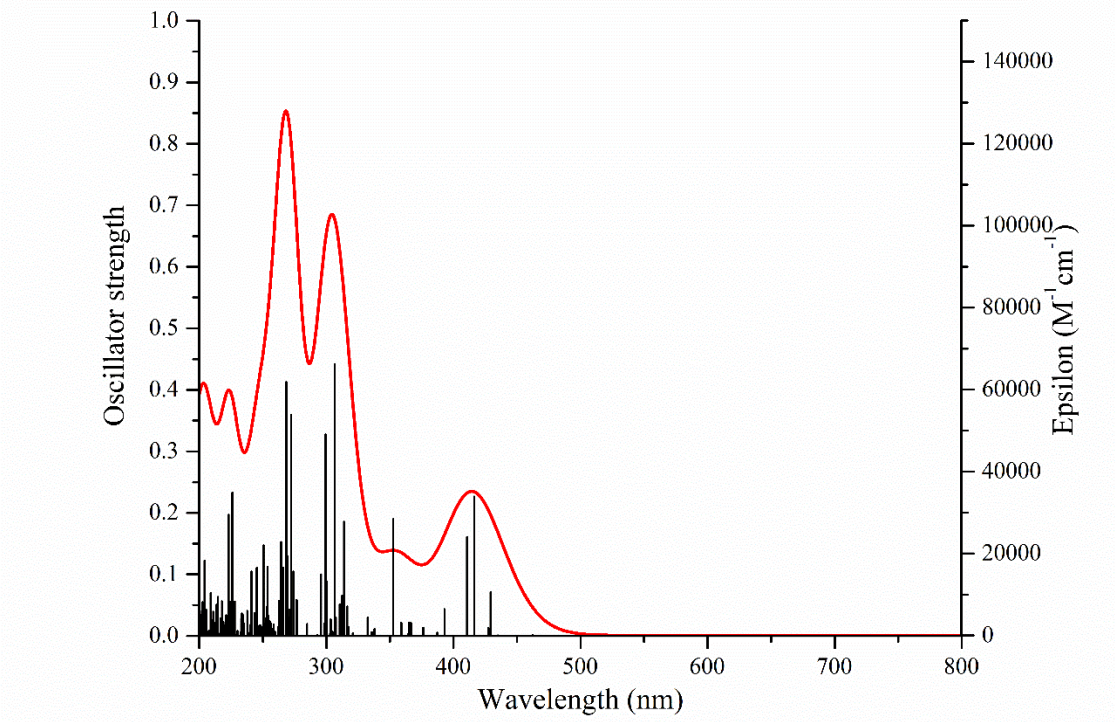

Figure S 20 TD-DFT simulated absorption spectrum of **[Ru(bpy)$_2$napp]$^{2+}$** in water.

Table Selected transitions from TD-DFT calculations of **$[Ru(bpy)_2napp]^{2+}$** in the singlet ground state in water.

Energy (eV)	λ (nm)	f	Major Transitions	Character
2.66	466	0.0001	HOMO→LUMO (23%), HOMO→L+1 (30%), HOMO→L+3 (40%)	$^1MLCT_{NAPP}$ (maj.) + $^1MLCT_{bpy}$
2.67	465	0.0002	HOMO→L+2 (92%)	$^1MLCT_{bpy}$
2.68	462	0.0018	HOMO→LUMO (60%), HOMO→L+1 (38%)	$^1MLCT_{NAPP}$ (maj.) + $^1MLCT_{bpy}$
2.85	435	0.0007	H-2→L+1 (23%), H-2→L+3 (20%), H-1→L+2 (49%)	$^1MLCT_{NAPP}$ + $^1MLCT_{bpy}$ (maj.)
2.89	429	0.0711	H-1→LUMO (67%), H-1→L+1 (24%)	$^1MLCT_{NAPP}$ + $^1MLCT_{bpy}$
2.90	427	0.0125	H-2→LUMO (74%), H-2→L+3 (11%), H-1→L+2 (11%)	$^1MLCT_{NAPP}$ (maj.) + $^1MLCT_{bpy}$
2.98	416	0.2264	H-2→L+2 (34%), H-1→LUMO (21%), H-1→L+1 (26%), H-1→L+3 (14%)	$^1MLCT_{NAPP}$ + $^1MLCT_{bpy}$ (maj.)
3.02	411	0.1607	H-2→L+1 (45%), H-2→L+3 (11%), H-1→L+2 (33%)	
3.15	393	0.0432	H-2→L+2 (26%), HOMO→L+4 (56%)	
3.20	387	0.0052	HOMO→LUMO (14%), HOMO→L+1 (27%), HOMO→L+3 (53%)	$^1MLCT_{NAPP}$ (maj.) + $^1MLCT_{bpy}$
3.30	376	0.013	H-2→L+2 (14%), H-1→L+1 (32%), H-1→L+3 (13%), HOMO→L+4 (24%)	
3.38	366	0.0211	H-2→L+3 (10%), H-2→L+4 (61%), H-1→L+3 (12%)	$^1MLCT_{NAPP}$ (maj.) + $^1LLCT_{bpy\rightarrow NAPP}$
3.40	365	0.0217	H-1→L+4 (81%)	
3.40	364	0.0034	H-2→LUMO (11%), H-2→L+1 (21%), H-2→L+3 (40%), H-2→L+4 (10%)	$^1MLCT_{NAPP}$ (maj.) + $^1MLCT_{bpy}$
3.45	359	0.0214	H-2→L+4 (22%), H-1→L+3 (31%), HOMO→L+4 (10%)	
3.52	353	0.1896	H-3→LUMO (38%), H-3→L+1 (21%), H-3→L+3 (10%), H-1→L+3 (11%)	$^1MLCT_{bpy}$ (maj.) + $^1LLCT_{NAPP\rightarrow bpy}$
3.67	338	0.011	H-4→LUMO (19%), H-4→L+1 (10%), H-3→LUMO (14%), H-3→L+4 (37%)	$^1MLCT_{bpy}$ + $^1LLCT_{NAPP\rightarrow bpy}$ (maj.)
3.69	336	0.0061	HOMO→L+5 (95%)	$^1MLCT_{bpy}$
3.73	332	0.0298	H-3→LUMO (18%), H-3→L+3 (47%)	$^1MLCT_{bpy}$ + $^1LLCT_{NAPP\rightarrow bpy}$ (maj.)
3.87	321	0.0043	H-3→L+1 (38%), H-3→L+3 (18%), H-1→L+5 (15%), HOMO→L+6 (12%)	$^1MLCT_{bpy}$ + $^1LLCT_{NAPP\rightarrow bpy}$
3.88	319	0.0004	H-3→L+1 (20%), H-1→L+5 (42%), HOMO→L+6 (23%)	
3.91	317	0.0143	H-2→L+5 (86%)	$^1MLCT_{bpy}$ (maj.) + $^1LLCT_{NAPP\rightarrow bpy}$
3.91	317	0.0043	H-1→L+5 (21%), HOMO→L+6 (44%), HOMO→L+7 (22%)	
3.92	316	0.0476	H-3→L+2 (79%)	$^1MLCT_{bpy}$ + $^1LLCT_{NAPP\rightarrow bpy}$ (maj.)
3.95	314	0.1854	H-4→LUMO (43%), H-4→L+3 (23%), H-3→L+4 (16%)	
3.97	312	0.0655	HOMO→L+8 (87%)	
3.99	310	0.0513	H-2→L+7 (12%), HOMO→L+7 (52%)	$^1MLCT_{bpy}$ (maj.) + $^1LLCT_{NAPP\rightarrow bpy}$
4.03	307	0.0299	H-1→L+6 (46%), HOMO→L+15 (18%)	
4.05	306	0.4414	H-4→L+1 (20%), H-4→L+3 (38%), H-3→L+4 (29%)	$^1MLCT_{bpy}$ + $^1LLCT_{NAPP\rightarrow bpy}$ (maj.)
4.07	305	0.0064	H-2→L+6 (35%), H-2→L+7 (10%), HOMO→L+15 (11%), HOMO→L+16 (19%)	$^1MLCT_{bpy}$ (maj.) + $^1LLCT_{NAPP\rightarrow bpy}$
4.09	303	0.0268	H-8→LUMO (12%), H-8→L+1 (11%), H-1→L+6 (10%), H-1→L+7 (17%), HOMO→L+15 (12%)	
4.09	303	0.0263	H-8→LUMO (23%), H-8→L+1 (21%), H-8→L+3 (18%)	$^1MLCT_{bpy}$ + $^1LLCT_{NAPP\rightarrow bpy}$ (maj.)
4.09	303	0.003	H-2→L+6 (29%), H-2→L+7 (20%), HOMO→L+16 (14%)	$^1MLCT_{bpy}$
4.13	300	0.0244	H-4→LUMO (12%), H-4→L+1 (52%), H-4→L+3 (18%)	$^1MLCT_{bpy}$ + $^1LLCT_{NAPP\rightarrow bpy}$ (maj.)
4.13	300	0.0891	H-4→L+4 (10%), H-1→L+6 (16%), H-1→L+7 (41%)	$^1MLCT_{bpy}$ (maj.) + $^1LLCT_{NAPP\rightarrow bpy}$

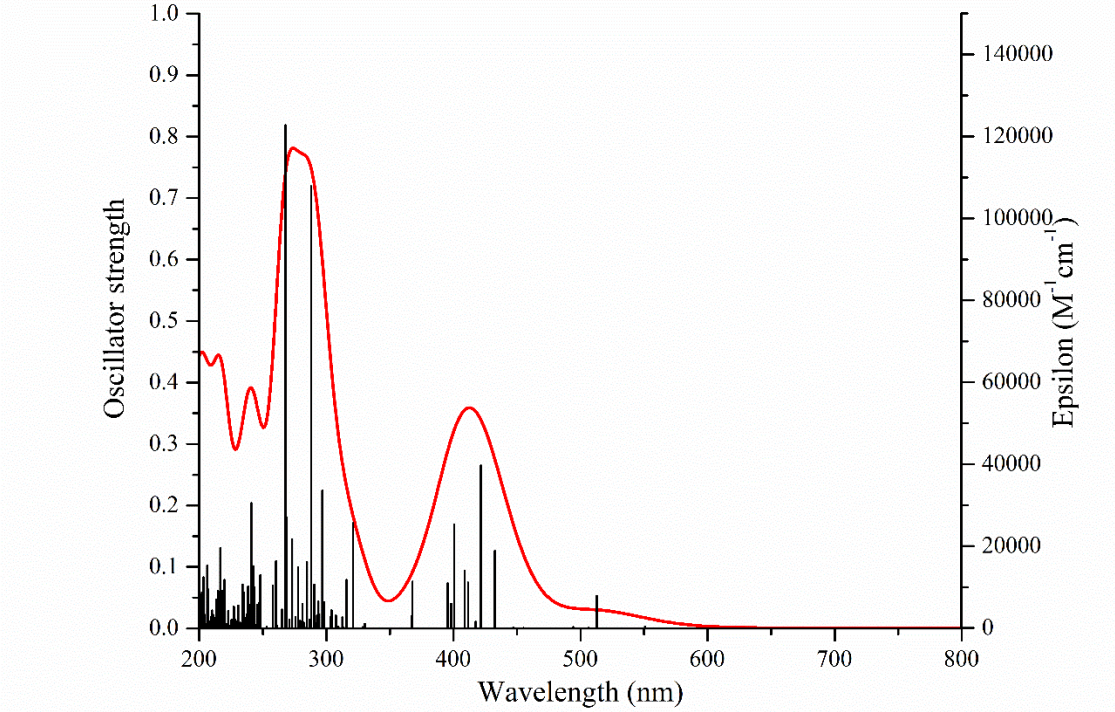

Figure S 21 TD-DFT simulated absorption spectrum of **[Ru(bpy)$_2$napp-H]$^{2+}$** in water.

Table Selected transitions from TD-DFT calculations of **[Ru(bpy)$_2$napp-H]$^{2+}$** in the singlet ground state in water.

Energy (eV)	λ (nm)	f	Major Transitions	Character
2.25	551	0.0030	HOMO→LUMO (93%)	
2.42	513	0.0529	H-1→LUMO (93%)	
2.45	507	0.0012	H-2→LUMO (90%)	$^1MLCT_{NAPP}$ (maj.) + $^1LLCT_{bpy\rightarrow NAPP}$
2.51	494	0.0023	HOMO→L+1 (64%), HOMO→L+2 (22%)	
2.72	455	0.0009	H-2→L+1 (53%), H-2→L+2 (19%), H-1→L+1 (12%)	
2.75	450	0.0004	HOMO→L+4 (86%)	$^1MLCT_{bpy}$ (maj.) + $^1MLCT_{NAPP}$
2.77	447	0.0013	HOMO→L+3 (89%)	
2.87	433	0.1261	H-1→L+1 (35%), HOMO→L+2 (22%)	$^1MLCT_{NAPP}$ (maj.) + $^1MLCT_{bpy}$
2.94	422	0.2652	H-1→L+1 (22%), HOMO→L+1 (16%), HOMO→L+2 (33%)	
2.97	417	0.0111	H-2→L+3 (26%), H-1→L+4 (44%)	$^1MLCT_{bpy}$ (maj.) + $^1MLCT_{NAPP}$
3.01	412	0.0745	H-3→LUMO (22%), H-2→L+3 (10%), H-2→L+4 (17%), H-1→L+3 (41%)	
3.03	409	0.0934	H-3→LUMO (58%), H-2→L+2 (11%), H-1→L+3 (10%)	$^1MLCT_{NAPP}$ (maj.) + $^1MLCT_{bpy}$
3.10	400	0.1690	H-2→L+2 (20%), H-2→L+3 (42%), H-1→L+4 (19%)	$^1MLCT_{bpy}$ (maj.) + $^1MLCT_{NAPP}$
3.11	398	0.0400	H-2→L+1 (25%), H-2→L+2 (35%), H-2→L+4 (12%)	
3.14	395	0.0737	H-1→L+1 (15%), H-1→L+2 (57%), H-1→L+4 (17%)	$^1MLCT_{NAPP}$ (maj.) + $^1MLCT_{bpy}$
3.37	368	0.0760	H-4→LUMO (75%)	
3.38	367	0.0195	H-4→LUMO (14%), H-2→L+4 (37%), H-1→L+3 (19%)	$^1MLCT_{bpy}$ (maj.) + $^1MLCT_{NAPP}$
3.73	333	0.0003	H-5→LUMO (94%)	$^1LLCT_{bpy\rightarrow NAPP}$
3.75	330	0.0073	HOMO→L+5 (91%)	$^1MLCT_{bpy}$ (maj.) + $^1MLCT_{NAPP}$
3.77	329	0.0019	H-6→LUMO (93%)	$^1LLCT_{bpy\rightarrow NAPP}$
3.86	321	0.1711	H-3→L+1 (81%)	$^1LLCT_{NAPP\rightarrow bpy}$

3.92	316	0.0791	H-7→LUMO (29%), H-3→L+2 (46%)	$^1MLCT_{bpy}$ (maj.) + $^1LLCT_{NAPP\rightarrow bpy}$
3.96	313	0.0011	H-1→L+5 (74%), HOMO→L+7 (12%)	$^1MLCT_{bpy}$
3.97	313	0.0178	H-2→L+5 (89%)	$^1MLCT_{bpy}$ (maj.) + $^1MLCT_{NAPP}$
3.99	311	0.0004	HOMO→L+7 (56%), HOMO→L+8 (10%)	$^1MLCT_{bpy}$
4.03	307	0.0209	HOMO→L+9 (40%), HOMO→L+16 (29%)	
4.08	304	0.0297	HOMO→L+7 (11%), HOMO→L+8 (29%), HOMO→L+9 (14%), HOMO→L+16 (10%)	
4.08	304	0.0172	H-1→L+7 (10%), HOMO→L+9 (32%), HOMO→L+17 (24%)	
4.09	303	0.0197	HOMO→L+8 (37%), HOMO→L+16 (11%), HOMO→L+17 (15%)	

Table Predicted phosphorescence energies employing different approaches.[a]

Complex	Theoretical[b]			Experimental
	λ_{TDDFT} (nm)	$\lambda_{0,0}$ (nm)	λ_{AE}(nm)	$\lambda_{em@298K}$ (nm)
[Ru (bpy)$_2$(NAPP)]$^{2+}$	540	529	1007	
[Ru (bpy)$_2$(NAPP-H)]$^{3+}$	568	780	860	

[a]λ_{TDDFT}= wavelength of $S_0\rightarrow T_1$ transition obtained by TDDFT at the S_0 optimized geometry. $\lambda_{0,0}$= 1240/[E(T_1)–E(S_0)] at their respective optimized geometries obtained by DFT. λ_{AE}= 1240/[E(T_1)–E(S_0)] at the T_1 optimized geometry (adiabatic electronic emission) obtained by DFT. All values were determined with H_2O as solvent.

8. DNA luminescence titration for $[Ru(bpy)_2napp]^{2+}$

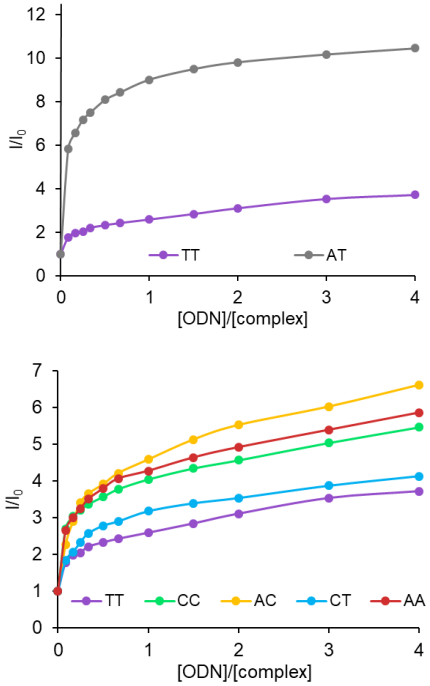

Figure S 22 Luminescence titration of **$[Ru(bpy)_2napp]^{2+}$** in the presence of well-matched and mismatched DNA hairpins oligonucleotides.

9. Circular dichroism melting curves

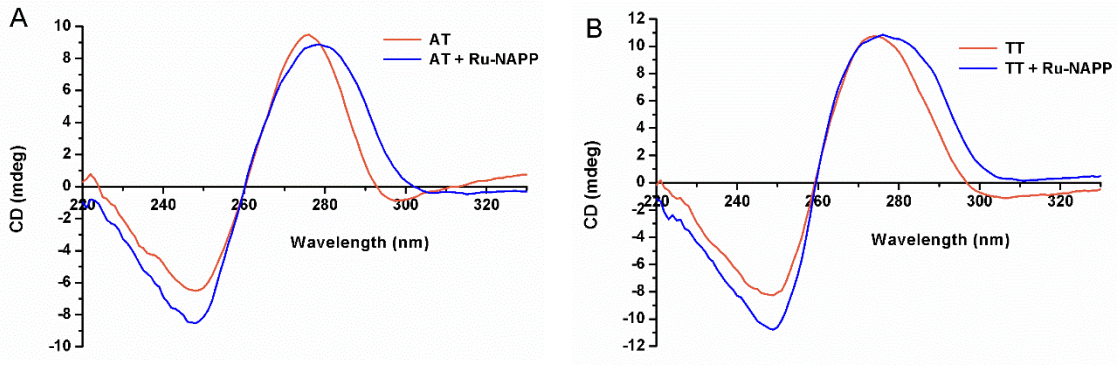

10.

Figure S 23 CD spectra of AT (A) and TT (B) hairpin duplex (in red) in Tris·HCl buffer 5 mM, NaCl 1 mM, pH 7.5 under ambient air condition in the presence of 1 eq. of **[Ru(bpy)$_2$napp]$^{2+}$** (in blue).

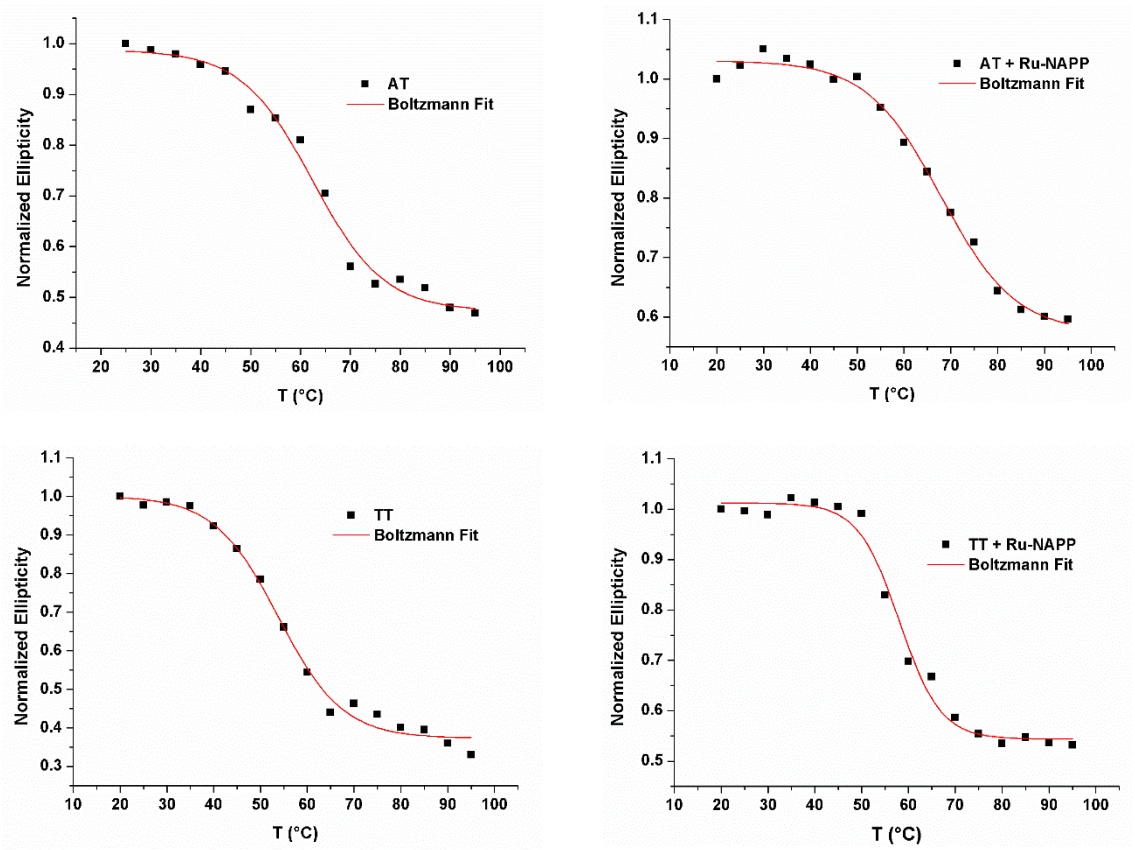

Figure S 24 Melting curves of AT and TT containing hairpins (1 eq.) in the absence and in the presence of **[Ru(bpy)$_2$napp]$^{2+}$** (+ **[Ru(bpy)$_2$napp]$^{2+}$**, 1 eq.).

11. Bio-Layer Interferometry data

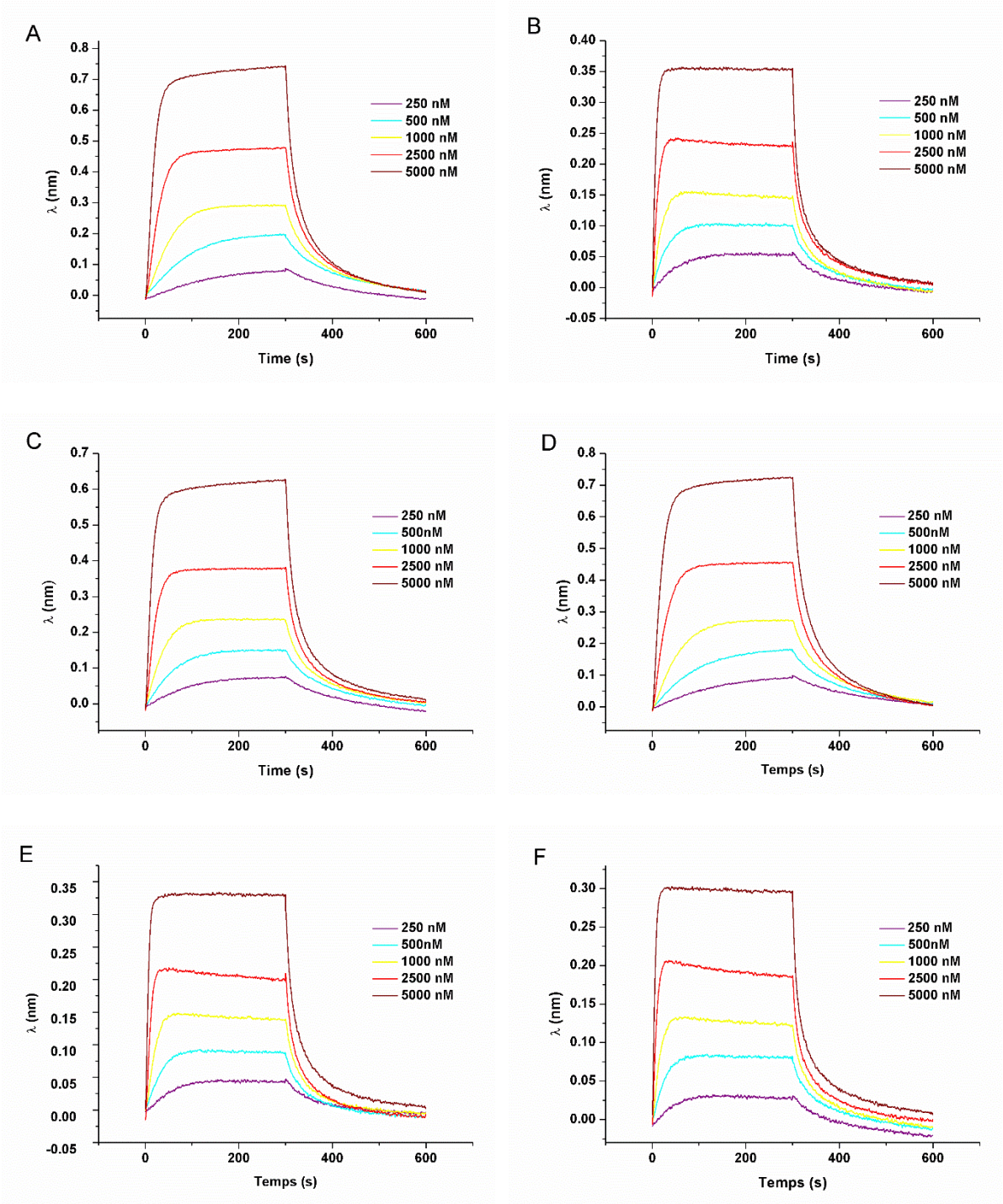

Figure S 25 BLI sensorgrams for the interaction of **[Ru(bpy)$_2$napp]$^{2+}$** with six different hairpins (A = AT, B = TT, C = AA, D = AC, E = CC, F = CT). The analyte concentrations were 250, 500, 1 000, 2 500, 5 000, 10 000 nM.

12. References

1

1. L. Jiang, X. Lu, H. Zhang, Y. Jiang and D. Ma, *J. Org. Chem.*, 2009, **74**, 4542-4546.
2. G. D. Vo and J. F. Hartwig, *J. Am. Chem. Soc.*, 2009, **131**, 11049-11061.
3. T. C. Bruice, *J. Am. Chem. Soc.*, 1957, **79**, 702-705.
4. A. S. Karpenko, M. O. Shibinskaya, N. M. Zholobak, Z. M. Olevinskaya, S. A. Lyakhov, L. A. Litvinova, M. Y. Spivak and S. A. Andronati, *Pharm. Chem. J.*, 2006, **40**, 595-602.
5. G. Reissenweber and D. Mangold, *Angew. Chem. Int. Ed.*, 1981, **20**, 882-883.
6. S. Ji, H. Guo, X. Yuan, X. Li, H. Ding, P. Gao, C. Zhao, W. Wu, W. Wu and J. Zhao, *Org. Lett.*, 2010, **12**, 2876-2879.
7. Q. Deraedt, L. Marcélis, T. Auvray, G. S. Hanan, F. Loiseau and B. Elias, *Eur. J. Inorg. Chem.*, 2016, **2016**, 3649-3658.